of H_2O_2 was added and, after an additional 8 h, 10 mL more of H_2O_2 was added. The solution was allowed to react for an additional 20 h and then NaN_3 (39 g, 0.6 mol) was added. The pH was adjusted to 7.5 with 1 M H_2SO_4 and the mixture was maintained at that pH by adding 1 M H_2SO_4 with a peristaltic pump. The solution was warmed to 30 °C for 14 h. GC analysis indicated a complete reaction. The methanol was removed under reduced pressure. After 100 mL of water was added, the solution was extracted with dichloromethane (150 mL × 3). The organic layer was washed with brine, dried over Na_2SO_4, and then evaporated to remove solvent. Hexane was added to precipitate benzamide. This mixture was filtered and the filtrate was evaporated under reduced pressure. The residue was dissolved in pyridine (36.4 mL) and reacted with acetic anhydride (34 mL, 360 mmol). After 3 h at room temperature, methanol (8 mL) was added to quench the excess acetic anhydride. Ethyl acetate (150 mL) was added, and then the resulting solution was washed with water (100 mL × 2), 1 N HCl (100 mL × 2), saturated $NaHCO_3$, and brine and then dried over Na_2SO_4. The solvent was removed under reduced pressure. Distillation of the residue yielded 52 g of **9** (76% based on acrolein diethyl acetal, bp 88-89 °C (0.4 mmHg)). ^1H NMR data are in agreement with that reported.[3a]

Resolution of Compound 9. Method A. A solution of **9** (2.31 g, 10 mmol) in 100 mL of phosphate buffer solution (0.05 M, pH 7) was mixed with 100 mg of lipoprotein lipase 80 from *Pseudomonas* (from Amano Co.) at room temperature with stirring. The pH was maintained at 7.0 with a peristaltic pump by adding 0.25 N NaOH and the degree of conversion was monitored by the consumption of base. After 50% conversion (12 h), the reaction mixture was extracted with ethyl acetate. The combined extracts were dried over anhydrous sodium sulfate and the solvent was removed in vacuo. The products were separated by silica gel column chromatography (ethyl acetate/*n*-hexane = 1:12 to 1:8) to give 1.06 g (46%) of **9a** ($[\alpha]^{25}_D$ -5.1° (*c* = 1.5, $CHCl_3$)) and 0.89 g (47%) of alcohol **10** ($[\alpha]^{25}_D$ +45.5° (*c* = 1.5, $CHCl_3$)). The R_f values of **9a** and **10** were 0.42 and 0.17 (ethyl acetate/*n*-hexane = 1:5), respectively. Compound **10**: ^1H NMR ($CDCl_3$/TMS) δ 1.23 (3 H, t, J = 7.1 Hz), 1.26 (3 H, t, J = 7.1 Hz), 2.47 (1 H, d, J = 6.0 Hz), 3.35 (1 H, dd, J = 6.0 Hz and 12.8 Hz), 3.51 (1 H, dd, J = 3.6 Hz and 12.8 Hz), 3.51 (1 H, dd, J = 3.6 Hz and 12.8 Hz), 3.60 (1 H, m), 3.77 (4 H, m), 4.47 (1 H, d, J = 6.2 Hz). The enantiomeric excess of **9a** was determined to be greater than 98% by ^1H NMR in the presence of $Eu(hfc)_3$ (24 mg). The relative intensities of the acetoxy group at 3.52 (major) and 3.57 (minor) were used for ee determination. On the other hand, compound **10** was treated with (+)-2-methoxy-2-(trifluoromethyl)phenylacetyl chloride and the resulting ester was analyzed by ^1H NMR to establish an ee of 97%. The relative intensities of the methine proton in the acetal group at 4.66 (d, major) and 4.54 (d, minor) were measured for ee determination.

Method B. The same substrate solution as described in method A was mixed with an immobilized lipase (prepared by stirring 100 mg of the enzyme and 5 g of XAD-8 (from Sigma) in 5 mL of 0.05 M phosphate, pH 7, overnight at 8 °C) at room temperature with stirring. The resulting solution was then treated in the same way as in method A. When the conversion reached 50% (5 h), the immobilized enzyme was removed by filtration and washed with dichloromethane (the immobilized enzyme recovered had 80% activity retained). The combined filtrate was separated and then the water layer was extracted with ethyl acetate to recover the product.

Hydrolysis of 9a and Determination of Stereochemistry. To a solution of **9a** (1.19 g) in 10 mL of methanol cooled with an ice water bath was added NaH (12 mg, 0.5 mmol). The solution was stirred for 30 min at the same temperature and then for 2 h at room temperature. After 10 mL of brine solution was added, the resulting mixture was extracted with dichloromethane. The organic layer was dried over anhydrous sodium sulfate. After removal of the solvent under reduced pressure, the residue was purified by silica gel column chromatography (ethyl acetate/*n*-hexane = 1:5) to give 0.916 g of a product which is the enantiomer of **10**. To generate the aldehyde, the acetal was treated with 0.1 N HCl according to the procedure described previously.[3a] The stereochemistry of **2** was determined on the basis of the product obtained after aldol reaction and reductive amination.

Acknowledgment. Support of this work at Texas A&M from NSF and NIH and that at MIT from BPEC is gratefully acknowledged. C.F.B. thanks the NSF for a predoctoral fellowship. C.v.d.O. acknowledges a Whitaker Health Sciences Fellowship for support.

2,4-Dimethylene-1,3-cyclobutanediyl, the Non-Kekulé Isomer of Benzene. Synthesis, EPR, and Electronic Spectroscopy

Gary J. Snyder[1] and Dennis A. Dougherty*

Contribution No. 7846 from the Arnold and Mabel Beckman Laboratory of Chemical Synthesis, 164-30, California Institute of Technology, Pasadena, California 91125.
Received September 22, 1988

Abstract: The preparation and direct observation of triplet 2,4-dimethylene-1,3-cyclobutanediyl (**1**), the non-Kekulé isomer of benzene, is described. The biradical was generated by photolysis of 5,6-dimethylene-2,3-diazabicyclo[2.1.1]hex-2-ene (**2**) (which was synthesized in several steps from benzvalene) under cryogenic, matrix isolation conditions. Biradical **1** was characterized by EPR spectroscopy ($|D/hc|$ = 0.0204 cm^{-1}, $|E/hc|$ = 0.0028 cm^{-1}) and found to have a triplet ground state. The Δm_s = 2 transition displays hyperfine splitting attributed to a 7.3-G coupling to the ring methine and a 5.9-G coupling to the exocyclic methylene protons. Several experiments, including application of the magnetophotoselection (mps) technique in the generation of biradical **1**, have allowed a determination of the zero-field triplet sublevels as x = -0.0040, y = +0.0136, and z = -0.0096 cm^{-1}, where x and y are, respectively, the long and short in-plane axes and z the out-of-plane axis of **1**. Triplet **1** is yellow-orange and displays highly structured absorption (λ_{max} = 506 nm) and fluorescence (λ_{max} = 510 nm) spectra, with vibronic spacings of 1520 and 620 cm^{-1} for absorption and 1570 and 620 cm^{-1} for emission. The spectra were unequivocally assigned to triplet **1** by the use of a novel technique that takes advantage of the biradical's photolability. The absorption has ϵ = 7200 M^{-1} cm^{-1} and f = 0.022, establishing that the transition is spin-allowed. Further use of the mps technique has demonstrated that the transition is x-polarized, and the excited state is therefore of B_{1g} symmetry, in accord with theoretical predictions.

A large variety of thermal and photochemical reactions are generally believed to involve biradicals as short-lived intermediates, proceed via biradical-like electronic states, or traverse transition structures envisioned as possessing biradical character.[2] While this has historically provided much of the motivation for the study of biradicals, the attention of investigators in the field has recently

(1) NSF predoctoral fellow, 1981-1984.

(2) (a) *Diradicals*; Borden, W. T., Ed.; Wiley: New York, 1982. (b) Wirz, J. *Pure Appl. Chem.* **1984**, *56*, 1289-1300. Dauben, W. G.; Salem, L.; Turro, N. J. *Acc. Chem. Res.* **1975**, *8*, 41-54. Bonacic-Koutecky, V.; Koutecky, J.; Michl, J. *Angew. Chem., Int. Ed. Engl.* **1987**, *26*, 170-189. Salem, L.; Rowland, C. *Angew. Chem., Int. Ed. Engl.* **1972**, *11*, 92-111.

0002-7863/89/1511-3927$01.50/0

shifted somewhat toward studying biradicals both as novel species in their own right and as potential building blocks for materials with unique magnetic, electrical, and optical properties.[3-5]

One factor that has contributed to this shift in focus is the finding that many delocalized hydrocarbon biradicals are relatively stable and amenable to direct study. Delocalized biradicals have been referred to as non-Kekulē molecules,[6] because their unpaired electrons are part of a classical π-system but are topologically prevented from forming a π-bond. A major goal of current work has been to acquire an understanding of the factors that govern stability and spin preference in these systems. Such insight could potentially allow the design of extended systems with many electrons whose mutual interactions are controlled topologically. For example, this idea has recently been applied both theoretically[4] and experimentally[5] to the construction of organic ferromagnets. In addition, the wealth of experimental data offered by delocalized biradicals provides valuable benchmarks for theoretical methods that profess to treat homolytic bond cleavage reactions accurately, and these species constitute important tests of electronic structure theory in a general sense.

The present work concerns a fundamentally unique non-Kekulē hydrocarbon, 2,4-dimethylene-1,3-cyclobutanediyl, alternatively 1,3-dimethylenecyclobutadiene, (**1**). Simple consideration of the

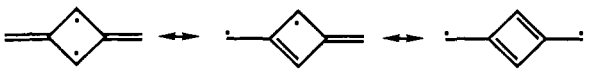

1

possible resonance structures for this non-Kekulē isomer of benzene reveals extensive delocalization of the unpaired electrons, placing spin density at both the ring methine and exocyclic methylene positions. Especially noteworthy are resonance structures that possess a cyclobutadiene moiety, perhaps suggesting an added dimension in the spectroscopy and reactivity of the biradical.

It should be noted at the outset that all competent theoretical models are in agreement that **1** should have a triplet ground state. For several non-Kekulē molecules the spin preferences predicted by various theoretical treatments are in conflict,[4b,7] and systems have been designed and synthesized as tests of these theoretical models.[8] Biradical **1** is not such a test case. The topology of its π-system places **1** in a class for which trimethylenemethane (TMM) is the prototype, and both are predicted to have a sub-

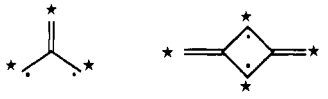

TMM 1

stantial, i.e., several kcalories per mole, triplet preference. For example, applying the "starred-unstarred" atom formalism,[9] each has two more starred atoms than unstarred. Ovchinnikov's rule, derived within the framework of valence bond theory,[4a] states that this should lead to a triplet ground state. Simple MO theory reveals that both TMM and **1** have degenerate or nearly degenerate nonbonding molecular orbitals (NBMO) and thus should be triplets by Hund's rule. In fact, a triplet ground state for **1** was predicted on this basis as early as 1952 by Roberts.[10] More recently, Borden and Davidson have pointed out that while NBMO topology can lead to violations of Hund's rule in certain cases (e.g., D_{4h} cyclobutadiene and, perhaps, tetramethyleneethane), the rule should hold for **1** and TMM.[11,12] The key to this argument is that in each of these systems the NBMOs are not disjoint (see below), and the singlets suffer energetically as a result.[11,12] These qualitative predictions of T << S for **1** have been confirmed by ab initio calculations,[13a] which place planar singlet **1** (^1A_g) 10–15 kcal/mol above the triplet ($^3B_{2u}$).

We describe herein the synthesis and spectroscopy of biradical **1**.[14] This structure has turned out to be surprisingly well-suited to a thorough spectroscopic study, and we have characterized the biradical by EPR and electronic spectroscopy. The EPR experiments have furnished information concerning the geometry and spin distribution in the biradical as well as the magnitude of the spin–spin dipolar coupling interaction along each of the molecular axes. The triplet biradical displays a strong electronic transition, and several experiments are presented that establish the nature of this transition.

The scope of the present paper is limited to the spectroscopic characterization of **1** in rigid media at cryogenic temperature. In the following paper,[15] we address the thermal and photochemical interconversion of triplet **1** and its covalent isomer, 2,4-dimethylenebicyclo[1.1.0]butane, and the novel reactivity of the latter.

Synthesis

The synthesis of diazene **2**, the immediate precursor to **1**, involved several steps, some of which were not straightforward, and is discussed in some detail here. Those more physically inclined may wish to move directly to the next section, which begins the discussion of the spectroscopy of **1**.

Extrusion of nitrogen from azoalkanes has proven to be a fairly general method of preparing biradicals and strained hydrocarbons[16] under a variety of conditions. In particular, biradicals of the TMM family have been generated from 1,2-diazenes both thermally and photochemically.[17,18] Thus, diazene **2** presented itself as potentially the best source of biradical **1**.

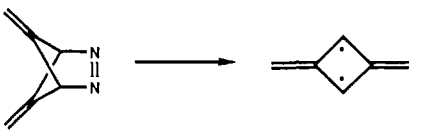

2 **1**

Our basic synthetic approach to **2** was motivated by the recent preparation of 2,3-diazabicyclo[2.1.1]hex-2-ene (**3**) and related

(3) See, for example: (a) Thomaides, J.; Maslak, P.; Breslow, R. *J. Am. Chem. Soc.* **1988**, *110*, 3970–3979. (b) LePage, T. J.; Breslow, R. *J. Am. Chem. Soc.* **1987**, *109*, 6412–6421. (c) Miller, J. S.; Epstein, A. J.; Reiff, W. M. *Acc. Chem. Res.* **1988**, *21*, 114–120. (d) Pranata, J.; Dougherty, D. A. *J. Am. Chem. Soc.* **1987**, *109*, 1621–1627. (e) Pranata, J.; Marudarajan, V. S.; Dougherty, D. A. *J. Am. Chem. Soc.* **1989**, *111*, 2026–2030. (f) Lahti, P. M.; Rossi, A. R.; Berson, J. A. *J. Am. Chem. Soc.* **1985**, *107*, 2273–2280. (g) Iwamura, H. *Pure Appl. Chem.* **1988**, *56*, 187–196.

(4) (a) Ovchinnikov, A. A. *Theor. Chim. Acta* **1978**, *47*, 297–304; *Dokl. Akad. Nauk. SSSR* **1977**, *236*, 928–931. (b) Klein, D. J.; Nelin, C. J.; Alexander, S.; Matsen, F. A. *J. Chem. Phys.* **1982**, *77*, 3101–3108.

(5) Torrance, J. B.; Oostra, S.; Nazzal, A. *Synth. Met.* **1987**, *19*, 709–714. See also: Korshak, Y. V.; Medvedeva, T. V.; Ovchinnikov, A. A.; Spector, V. N. *Nature* **1987**, *326*, 370–372.

(6) Dewar, M. J. S. *The Molecular Orbital Theory of Organic Chemistry*; McGraw-Hill: New York, 1969; pp 232–233.

(7) See, for example: (a) Dowd, P.; Chang, W.; Paik, Y. H. *J. Am. Chem. Soc.* **1987**, *109*, 5284–5285; **1986**, *108*, 7416–7417. (b) Du, P.; Borden, W. T. *J. Am. Chem. Soc.* **1987**, *109*, 930–931. (c) Du, P.; Hrovat, D. A.; Borden, W. T.; Lahti, P. M.; Rossi, A. R.; Berson, J. A. *J. Am. Chem. Soc.* **1986**, *108*, 5072–5074. (d) Roth, W. R.; Langer, R.; Bartmann, M.; Stevermann, B.; Maier, G.; Reisenauer, H. P.; Sustmann, R.; Müller, W. *Angew. Chem., Int. Ed. Engl.* **1987**, *26*, 256–258. (e) Du, P.; Hrovat, D. A.; Borden, W. T. *J. Am. Chem. Soc.* **1986**, *108*, 8086–8087.

(8) Seeger, D. E.; Lahti, P. M.; Rossi, A. R.; Berson, J. A. *J. Am. Chem. Soc.* **1986**, *108*, 1251–1265. Seeger, D. E.; Berson, J. A. *J. Am. Chem. Soc.* **1983**, *105*, 5144–5146.

(9) Longuet-Higgins, H. C. *J. Chem. Phys.* **1950**, *18*, 265–274.

(10) Roberts, J. D.; Streitwieser, A., Jr.; Regan, C. M. *J. Am. Chem. Soc.* **1952**, *74*, 4579–4582.

(11) Borden, W. T.; Davidson, E. R. *J. Am. Chem. Soc.* **1977**, *99*, 4587–4594.

(12) Borden, W. T. In ref 2a, Chapter 1, pp 1–72.

(13) (a) Feller, D.; Davidson, E. R.; Borden, W. T. *J. Am. Chem. Soc.* **1982**, *104*, 1216–1218. (b) Davidson, E. R.; Borden, W. T.; Smith, J. *J. Am. Chem. Soc.* **1978**, *100*, 3299–3302.

(14) Some aspects of this work have appeared in preliminary form: (a) Snyder, G. J.; Dougherty, D. A. *J. Am. Chem. Soc.* **1985**, *107*, 1774–1775; (b) **1986**, *108*, 299–300.

(15) Snyder, G. J.; Dougherty, D. A. *J. Am. Chem. Soc.*, following paper in this issue.

(16) Engel, P. S. *Chem. Rev.* **1980**, *80*, 99–150. Adam, W.; DeLucchi, O. *Angew. Chem., Int. Ed. Engl.* **1980**, *19*, 762–779. Meier, H.; Zeller, K.-P. *Angew. Chem., Int. Ed. Engl.* **1977**, *16*, 835–851.

(17) Berson, J. A. In ref 2a, Chapter 4, pp 151–194.

(18) Dowd, P. *Acc. Chem. Res.* **1972**, *5*, 242–248.

structures in our laboratory.[19] The key step in this synthesis was the thermal cycloaddition of methyl- or phenyltriazolinedione (MTAD or PTAD) across the central bond of bicyclo[1.1.0]butane (**4**) (eq 1). Standard methodology was then used to convert the

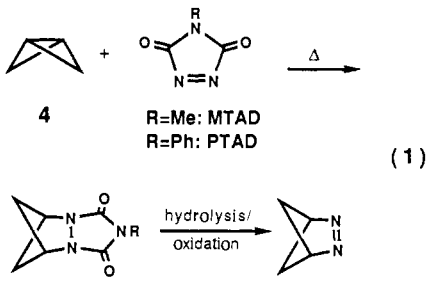

resulting urazole **5** to **3**.[19] In addition, accompanying our initial publication of this reaction, Amey and Smart reported gaining entry into the ring system of **5** by thermal and photochemical additions of MTAD and PTAD to various bridgehead-disubstituted bicyclobutanes.[20] We expected, therefore, that a triazolinedione (TAD) could be added to a bicyclobutane bearing substituents that would later allow introduction of the diene functionality of **2** (eq 2).

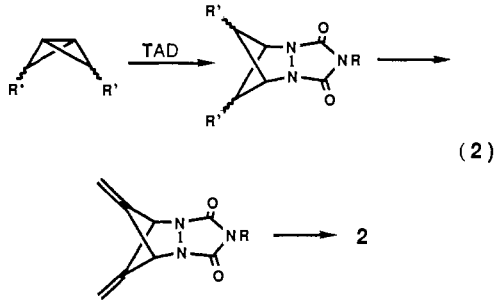

At the outset of our synthesis we found that the only available bicyclobutanes with useful functionality at only the 2- and 4-positions were those recently prepared from benzvalene by Christl and co-workers.[21,22] Thus, reductive ozonolysis of benzvalene yields **6** (Scheme I), whose hydroxyl groups can be protected to provide **7**. We had earlier shown[19,23] that the addition of TAD to bicyclobutane occurs from the endo direction.[24] Anticipating that the endo substituents of **7** would sterically hinder this process, we developed an alternative sequence (Scheme I) which afforded exo-substituted bicyclobutane **8**. Dibromide **9**, the product of formal addition of Br_2 across the transannular bond of benzvalene, was prepared by the method of Roth and Katz.[25] Ozonolytic cleavage of the double bond and subsequent "deprotection" of the bicyclobutane by *t*-BuLi coupling[26] afforded primarily the thermodynamically more stable[27] exo,exo epimer **8**; by ^{1}H NMR only about 5% of **7** was formed.[28]

Scheme I[a]

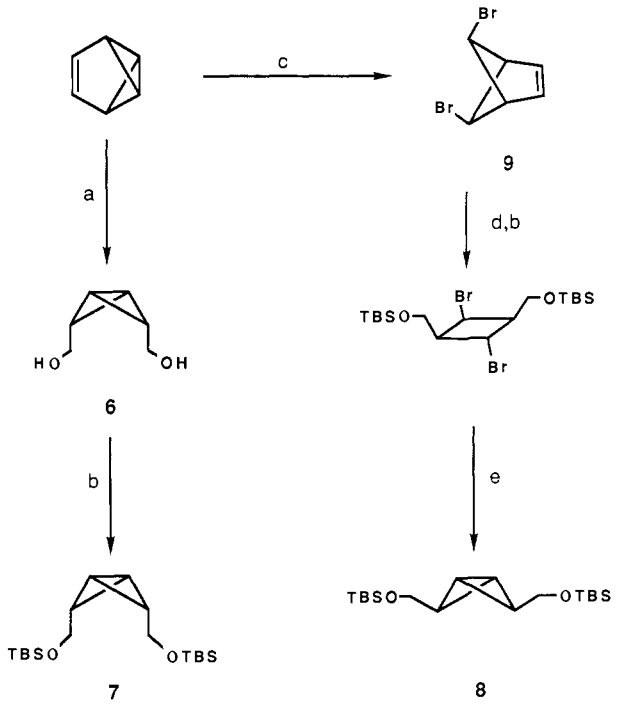

[a] Conditions: (a) O_3, −78 °C; $LiAlH_4$, THF, −30 °C (ref 21); (b) *t*-$BuMe_2SiCl$, imidazole, CH_2Cl_2; (c) Br_2, CCl_4/Et_2O, 0 °C (ref 25); (d) O_3, CH_2Cl_2, −78 °C; $LiAlH_4$, THF/Et_2O, 35 °C; (e) *t*-BuLi, Et_2O/pentane, −78 °C, Ar.

As expected, thermal addition of TAD to **8** was rapid, but **7** was completely inert toward comparable reaction conditions. However, even under conditions that had previously been found optimal for the formation of **5** (eq 1),[19] the product of the addition to **8** was unfortunately not a cycloadduct analogous to **5**. Instead, an intractable mixture of products with broad ^{1}H NMR signals, most notably one in the olefinic region, was obtained.

We have found, however, that MTAD adds *photochemically* to **7** to provide **10** in 37% yield after chromatography. The stereochemical assignment is firmly established by the observation of a 1.7-Hz coupling between the bridgehead (H_b) and endo (H_n)[30] protons; the exo protons of the endo,endo epimer (**13**; Scheme II) would not be expected to couple to H_b.[31] The mechanistic implication of this stereochemistry is that of *endo* attack by photochemically activated MTAD (MTAD*). This result suggested that MTAD* was taking the course expected for the thermal attack on **7** yet overcoming the steric hindrance that foiled our initial attempts at the thermal addition. Upon reinvestigating the failed thermal addition, we found that both MTAD and PTAD

(19) Chang, M. H.; Jain, R.; Dougherty, D. A. *J. Am. Chem. Soc.* **1984**, *106*, 4211-4217. Chang, M. H.; Dougherty, D. A. *J. Org. Chem.* **1981**, *46*, 4092-4093.

(20) Amey, R. L.; Smart, B. E. *J. Org. Chem.* **1981**, *46*, 4090-4092.

(21) (a) Leininger, H.; Lanzendörfer, F.; Christl, M. *Chem. Ber.* **1983**, *116*, 669-680. (b) Leininger, H.; Christl, M. *Angew. Chem., Int. Ed. Engl.* **1980**, *19*, 458-459. (c) Leininger, H.; Christl, M.; Wendisch, D. *Chem. Ber.* **1983**, *116*, 681-689.

(22) The preparation of 2,4-dicarbomethoxybicyclobutane has been reported by: Kelley, F. W., Jr. Ph.D. Thesis, University of Idaho, 1969. However, the reported procedure did not provide viable material in our hands. This bicyclobutane derivative has also been prepared electrochemically: Vellturo, A. F.; Griffin, G. W. *J. Org. Chem.* **1966**, *31*, 2241-2244.

(23) Chang, M. H.; Dougherty, D. A. *J. Am. Chem. Soc.* **1982**, *104*, 1131-1132.

(24) Such backside attack on strained σ-bonds is well precedented: Gassman, P. G. *Acc. Chem. Res.* **1971**, *4*, 128-136.

(25) Roth, R. J.; Katz, T. J. *J. Org. Chem.* **1980**, *45*, 961-965; *J. Am. Chem. Soc.* **1972**, *94*, 4770-4771. Roth, R. J. *Synth. Commun.* **1979**, *9*, 751-756.

(26) Christl, M.; Lang, R.; Herzog, C. *Tetrahedron* **1986**, *42*, 1585-1596. Christl, M.; Lang, R. *J. Am. Chem. Soc.* **1982**, *104*, 4494-4496.

(27) *exo,exo*-2,4-Dimethylbicyclobutane has been calculated to be ca. 13 kcal/mol more stable than its endo,endo counterpart: Richtsmeier, S. C.; Gassman, P. G.; Dixon, D. A. *J. Org. Chem.* **1985**, *50*, 3111-317.

(28) Quite consistent with the stereochemical assignments is the characteristic[29] upfield NMR shift of the endo protons of **8** (δ 1.13) relative to the exo protons of **7** (δ 2.70).

(29) Wiberg, K. B. *Adv. Alicyclic Chem.* **1968**, *2*, 185. Leftin, J. H.; Gil-Av, E.; Pines, A. *J. Chem. Soc., Chem. Commun.* **1968**, 396-397.

(30) Our previous exo-endo designation[19,23] was based on the bicyclo[2.1.1]hexane (or tricyclo[5.1.1.$0^{2,6}$]nonane) ring system; however, IUPAC rules dictate that these labels be reversed when heteroatoms are incorporated into the large bridge, as in **3**, **5**, **10**, etc. This nomenclature change does *not* constitute a change in assignment from the previous one.[14,19,23] *Nomenclature of Organic Compounds*; Fletcher, J. H., Dermer, O. C., Fox, R. B., Eds.; Advances in Chemistry 126; American Chemical Society: Washington, DC, 1974; pp 114-117.

(31) This coupling pattern is dependent on the proton-proton dihedral angles, which are essentially invariant because the ring system is so rigid. The coupling described is displayed in **5**[19] as well as many bicyclo[2.1.1]hexane derivatives: Wiberg, K. B.; Lowry, B. R.; Nist, B. J. *J. Am. Chem. Soc.* **1962**, *84*, 1594-1597.

Scheme II

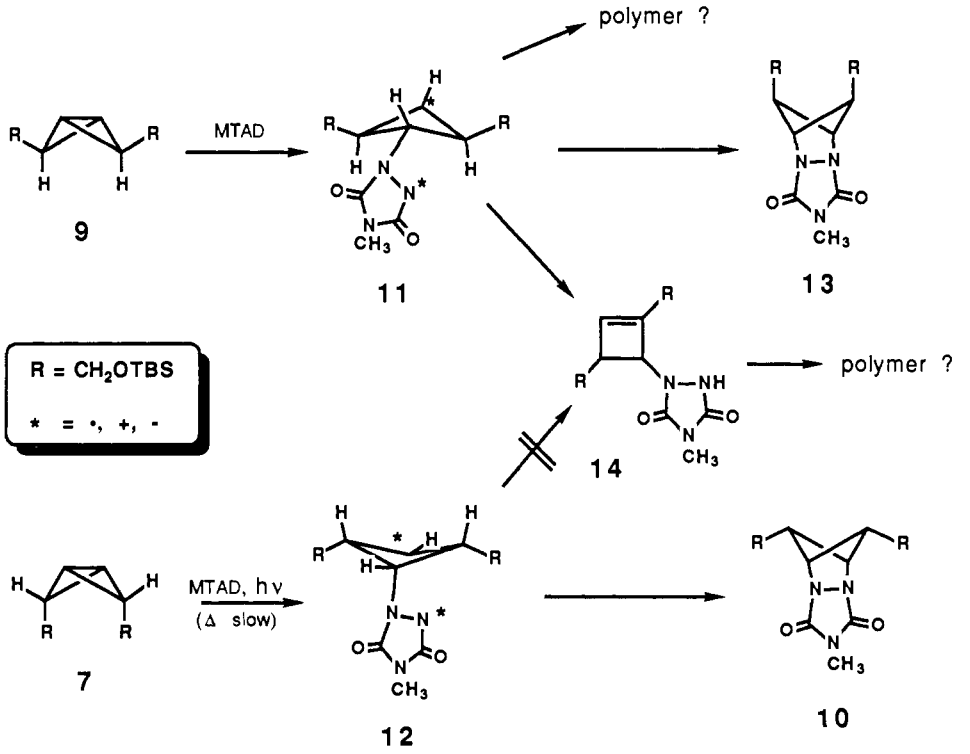

can be forced to cycloadd to **7** (isooctane, 100 °C), to form **10** and its *N*-phenyl analogue, respectively, albeit in yields estimated as 5% or less,

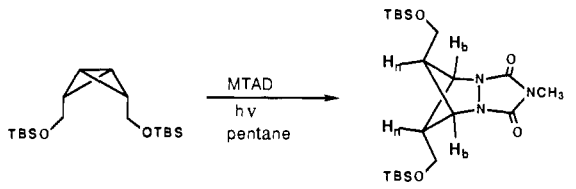

The differing reactions of **7** and **8** with TAD can be rationalized in a straightforward way. It is well established[24] that the endo addition to bicyclobutanes is stepwise, involving a zwitterionic or biradical-like intermediate (Scheme II).[19,32] We interpret the contrasting results of thermal addition of TAD to **8** and photochemical addition to **7** in terms of **11** and **12**, respectively, as shown in Scheme II. It is clear that the cyclobutyl ring of **11** will pucker so that all three substituents occupy pseudoequatorial positions. Closure to **13** then requires a ring flip and the concomitant development of close, nonbonded contacts between the siloxymethyl (R) groups. Additionally, the β-hydrogens in **11** are situated such that they can easily be abstracted by the neighboring divalent nitrogen to form an "ene" product, **14**. Whether the pathway to **14** traverses **11** or is concerted,[34] this process remains stereochemically viable. Analogues of **14** have been observed in the reactions of TAD with bicyclobutanes,[20] and although we have made no attempt to isolate such adducts, the observation of a broad olefinic ^{1}H NMR resonance suggests that such a process may be occurring. In contrast to the tribulations of **11**, intermediate **12** seems far more prone to cyclization. Specifically, puckering of the cyclobutyl ring so as to minimize steric repulsions also places the urazolyl group in a favorable position for closure to **10**. In addition, the β-hydrogens of **12** are not accessible for abstraction to give "ene"-type products.

We can cite two possible mechanisms for the photochemical attack of MTAD on **7**. Visible excitation of MTAD produces an n,π* state, leaving the azo moiety with free-radical character.[35] In fact, free-radical reactions are frequently observed in MTAD photochemistry.[36] Apparently, MTAD* (either singlet or triplet[37]) is much more reactive toward **7** than ground-state MTAD and can overcome the steric blockade presented by the siloxymethyl groups to form **12**. Alternatively, the initial step could be electron transfer,[38] as in the photochemical singlet addition of MTAD to naphthalene.[37] Collapse of the radical ion pair to form **12** would probably be less sensitive to steric hindrance than the thermal attack.

The conversion of **10** to diazene **2** was then a matter of introducing the double bonds and converting the urazole to the azo group. Removal of the TBS groups and transformation of the diol **15** to the corresponding dimesylate **16a**, dibromide **16b**, and diiodide **16c** was easily accomplished. However, the desired elimination could not be effected by the usual methods (*t*-BuO$^-$, DBU, AgF). We therefore turned to selenoxide chemistry. In

(32) Evidence for a zwitterionic intermediate in the addition of PTAD to vinyl ethers has been presented: Hall, J. H.; Jones, M. L. *J. Org. Chem.* **1983**, *48*, 822–826. Although, in general, the addition of TAD to olefins is thought to proceed via an aziridinium intermediate,[33] the intervention of a similar species is improbable in the present case. The potentially viable routes for TAD additions to olefins have been discussed.[33a] See also: Reference 24.

(33) (a) Adam, W.; Carballeira, N. *J. Am. Chem. Soc.* **1984**, *106*, 2874–2882. Cheng, C.-C.; Seymour, C. A.; Petti, M. A.; Greene, F. D.; Blount, J. F. *J. Org. Chem.* **1984**, *49*, 2910–2916. (b) Nelsen, S. F.; Kapp, D. L. *J. Am. Chem. Soc.* **1985**, *107*, 5548–5549.

(34) See, for example: Hoye, T. R.; Bottorff, K. J.; Caruso, A. J.; Dellaria, J. F. *J. Org. Chem.* **1980**, *45*, 4287–4292.

(35) Pocius, A. V.; Yardley, J. T. *J. Am. Chem. Soc.* **1973**, *95*, 7211–7251; *J. Chem. Phys.* **1974**, *61*, 2779–2792.

(36) Hall, J. H. *J. Org. Chem.* **1983**, *48*, 1708–1712. Pirkle, W. H.; Stickler, J. C. *J. Am. Chem. Soc.* **1970**, *92*, 7497–7499. Wamhoff, H.; Wald, K. *Chem. Ber.* **1977**, *110*, 1699–1715. See also: Hall, J. H.; Bigard, W. E.; Fargher, J. M.; Jones, M. L. *J. Org. Chem.* **1982**, *47*, 1459–1462.

(37) Kjell, D. P.; Sheridan, R. S. *J. Photochem.* **1985**, *28*, 205–213; *J. Am. Chem. Soc.* **1984**, *106*, 5368–5370.

(38) Such an electron transfer appears to be energetically feasible. By applying the Weller equation as suggested by Kjell and Sheridan,[37] and substituting an estimate of the oxidation potential for **7** of 1.67 V,[39] electron transfer from **7** to ^{1}MTAD* is found to be exothermic by ca. 4 kcal mol^{-1} (cf. transfer from naphthalene ($E^{ox}_{1/2}$ = 1.71 V), which is calculated to be exothermic by 2-3 kcal/mol[37]).

(39) This value was approximated as the oxidation potential for *endo,endo*-2,4-dimethylbicyclobutane, obtained from an empirical correlation between calculated IP and experimental oxidation potentials: Gassman, P. G.; Mullins, M. J.; Richtsmeier, S.; Dixon, D. A. *J. Am. Chem. Soc.* **1979**, *101*, 5793–5797.

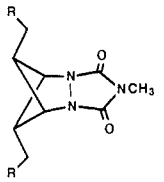

15 R = OH
16 a R = OSO_2CH_3
b R = Br
c R = I

particular, *o*-nitrophenyl selenoxide elimination[40] is reported to be the preferred method for the elimination in normally uncooperative primary isobutyl-type systems[40b] such as the present one. Conversion of selenide **17** (Scheme III) to the diene **18** was accomplished in 66% isolated yield.

We initially attempted to prepare **2** by subjecting urazole **18** to the standard hydrolysis/oxidation procedures.[41] These can involve either a mild basic hydrolysis to a semicarbazide[42] or more forcing hydrolysis to a hydrazine.[43] Either product can then be oxidized with cupric halides to copper complexes of the diazene.[41,42] These procedures were uniformly unsuccessful with **2**. We suspected that the strain present in the bicyclo[2.1.1] ring system might have been contributing not only to the anticipated thermal instability of **2** but also to the lability of the various intermediates in the hydrolysis/oxidation sequence. We therefore directed our attention toward carrying out the conversion under milder hydrolytic conditions and/or making the diazene at very low temperature.

Partial hydrolysis of **18** to the semicarbazide **19** (Scheme III)[42] proceeded at room temperature in ca. 90% yield after purification by preparative TLC. We were unaware of any method for very low temperature (−78 °C) conversion of a semicarbazide to a diazene. However, we found that treatment of a solution of the semicarbazide **19** in CH_2Cl_2 with MnO_2[43,44] at −78 °C for several hours converted a small amount of **19** to **2** as determined by ^1H NMR (see below). Encouraged by this result and the success of Dervan and co-workers in the heterogeneous, low-temperature preparation of 1,1-diazenes by treating hydrazine precursors with nickel peroxide,[45] we decided to try this reagent for the desired oxidation. Thus, treatment of **19** in CH_2Cl_2 with nickel peroxide at −78 °C results in a conveniently rapid[46] loss of **19**, as indicated by TLC analysis of the reaction mixture. Removal of the black oxidant by filtration and the solvent under vacuum at −78 °C affords diazene **2** as a white solid.

The ^1H NMR spectrum of **2** in CD_2Cl_2 reveals singlets at δ 5.48 and 4.75 in a 1:2 ratio. Diazene **2** also displays the characteristic azo group n,π^* transition at 331 nm (CD_2Cl_2, ϵ = 240 M^{-1} cm^{-1}; λ_{max} = 333 nm in MTHF). This transition energy is quite similar to that of **3** and its derivatives.[19,47]

Diazene **2** is quite labile thermally and loses nitrogen with first-order kinetics, which can be monitored by ^1H NMR between −40 and −70 °C. This decomposition affords 2,4-dimethylenebicyclo[1.1.0]butane (**20**), which is observable by ^1H NMR. Compound **20** dimerizes in the same temperature range, producing

20 21 22

two stable products, **21** and **22**.[48] The solution-phase thermal chemistry and photochemistry of **2** and **20**, as well as the spectroscopic characterization of the latter, are the subject of a separate paper[15] and will not be discussed here in any greater detail. We do note, though, that because thermal decomposition of **2** is so facile, samples of the diazene invariably contain ca. 30% of **20**–**22**. Most of the decomposition presumably occurs during transfer of cold (−78 °C) solutions of **2**, especially when these solutions are small in volume. ^1H NMR analysis of a typical sample implies that the nickel peroxide oxidation produces diazene **2** in an overall yield of ca. 35%, based on the amount of **2** and **20**–**22** present. Aside from these decomposition products, the diazene samples normally appear to be exceptionally clean. The oxidation byproducts presumably adhere to the nickel peroxide or are removed along with the reaction solvent.

More recently, nickel peroxide has been demonstrated to be generally useful for the preparation of 1,2-diazenes from phenyl[49] and methyl[47,50,51] semicarbazides. We note, though, that these reactions—especially those requiring temperatures as low as −78 °C—require a highly active form of nickel peroxide (see Experimental Section). Although we have no evidence concerning the mechanisms of these reactions, we assume they involve free-radical paths, as proposed in other nickel peroxide reactions.[52]

Finally, we required deuterium-labeled diazene for various spectroscopic and chemical studies to be described below and in the accompanying paper.[15] The bridgehead protons of bicyclobutanes are moderately acidic and can easily be exchanged for deuterium by treatment with alkyllithium followed by D_2O.[53] Accordingly, **7** was treated with *n*-BuLi and then D_2O three times in order to thoroughly wash out the bridgehead H. Completion of the synthetic sequence afforded **2**-d_2 with >99% bridgehead deuterium incorporation.

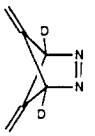

2-d_2

EPR Spectroscopy

When a frozen solution of diazene **2** in 2-methyltetrahydrofuran (MTHF) is irradiated directly (or triplet-photosensitized) with UV light in the cavity of an EPR spectrometer at 4–140 K, the spectrum of Figure 1 is observed.[14] This spectrum is characteristic of a randomly oriented ensemble of immobilized triplet species[54,55] and is described by zero-field splitting (zfs) parameters $|D/hc|$ = 0.0204 cm^{-1} and $|E/hc|$ = 0.0028 cm^{-1}.[56] Given its method

(40) (a) Sharpless, K. B.; Young, M. W. *J. Org. Chem.* **1975**, *40*, 947–949. (b) Reich, H. J.; Wollowitz, S.; Trend, J. E.; Chow, F.; Wendelborn, D. F. *J. Org. Chem.* **1978**, *43*, 1697–1705. Clive, D. L. J. *Tetrahedron* **1978**, *34*, 1049–1132.

(41) See, for example: Adam, W.; DeLucchi, O.; Erden, I. *J. Am. Chem. Soc.* **1980**, *102*, 4806–4809. Martin, M.; Roth, W. R. *Chem. Ber.* **1969**, *102*, 811–814. Cookson, R. C.; Gilani, S. S. H.; Stevens, I. D. R. *J. Chem. Soc. C* **1967**, 1905–1909. See also: Reference 19.

(42) Jösel, R.; Schröder, G. *Liebigs Ann. Chem.* **1980**, 1428–1437. Heyman, M.; Bandurco, V. T.; Snyder, J. P. *J. Chem. Soc., Chem. Commun.* **1971**, 297–298.

(43) See, for example: James, D. R.; Birnberg, G. H.; Paquette, L. A. *J. Am. Chem. Soc.* **1974**, *96*, 7465–7473. Wingard, R. E., Jr.; Russell, R. K.; Paquette, L. A. *J. Am. Chem. Soc.* **1974**, *96*, 7474–7482.

(44) Askani, R.; Wieduwilt, M. *Chem. Ber.* **1976**, *109*, 1887–1897. Berson, J. A.; Olin, S. S. *J. Am. Chem. Soc.* **1970**, *92*, 1086–1087.

(45) Dervan, P. B.; Squillacote, M. E.; Lahti, P. M.; Sylwester, A. P.; Roberts, J. D. *J. Am. Chem. Soc.* **1981**, *103*, 1120–1122. Duan, D. C.; Dervan, P. B. *J. Org. Chem.* **1983**, *48*, 970–976.

(46) The reaction requires less than 15 min if the nickel peroxide is sufficiently active (see Experimental Section).

(47) (a) Jain, R.; Sponsler, M. B.; Coms, F. D.; Dougherty, D. A. *J. Am. Chem. Soc.* **1988**, *110*, 1356–1366. (b) Jain, R.; Snyder, G. J.; Dougherty, D. A. *J. Am. Chem. Soc.* **1984**, *106*, 7294–7295.

(48) Photolysis of these dimers produces neither the EPR nor the optical spectra to be discussed below.

(49) Burger, U.; Mentha, Y.; Thorel, J. P. *Helv. Chim. Acta* **1986**, *69*, 670–675. Gleiter, R.; Zimmermann, H.; Sander, W.; Hauck, M. *J. Org. Chem.* **1987**, *52*, 2644–2653.

(50) Kaisaki, D. A.; Dougherty, D. A. *Tetrahedron Lett.* **1987**, *28*, 5263–5266. Coms, F. D.; Dougherty, D. A. *Tetrahedron Lett.* **1988**, *29*, 3753–3756.

(51) See also the low-temperature oxidation of hydrazines: Dowd, P.; Paik, Y. H. *Tetrahedron Lett.* **1986**, *27*, 2813–2816; and ref 7a.

(52) George, M. V.; Balachandran, K. S. *Chem. Rev.* **1975**, *75*, 491–519. Terabe, S.; Konaka, R. *J. Am. Chem. Soc.* **1969**, *91*, 5655–5657. Konaka, R.; Terabe, S.; Kuruma, K. *J. Org. Chem.* **1969**, *34*, 1334–1337.

(53) Closs, G. L.; Closs, L. E. *J. Am. Chem. Soc.* **1963**, *85*, 2022–2023.

(54) Wertz, J. E.; Bolton, J. R. *Electron Spin Resonance: Elementary Theory and Practical Applications*; McGraw-Hill: New York, 1972, Chapter 10, pp 223–257.

(55) Dougherty, D. A. In *Kinetics and Spectroscopy of Carbenes and Biradicals*; Platz, M. S., Ed.; Plenum Press: New York, in press.

(56) The error in each of these values is estimated as ±0.0003, by spectral simulation: see ref 57.

Scheme III[a]

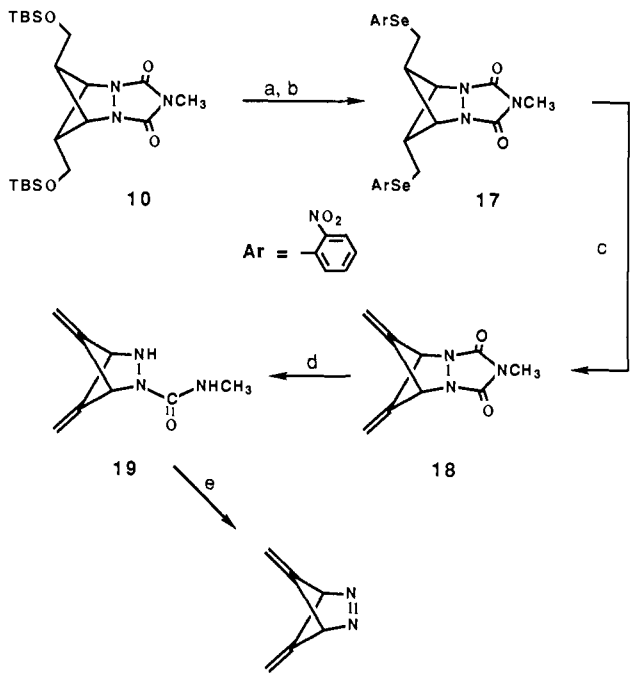

[a] Conditions: (a) n-$Bu_4N^+F^-$, THF; (b) o-$NO_2PhSeCN$, n-Bu_3P, THF; (c) O_3, $CHCl_3$, −60 °C; i-Pr_2NH, CCl_4, Δ; (d) KOH, DMSO/H_2O (6:1); (e) nickel peroxide, CH_2Cl_2, −78 °C.

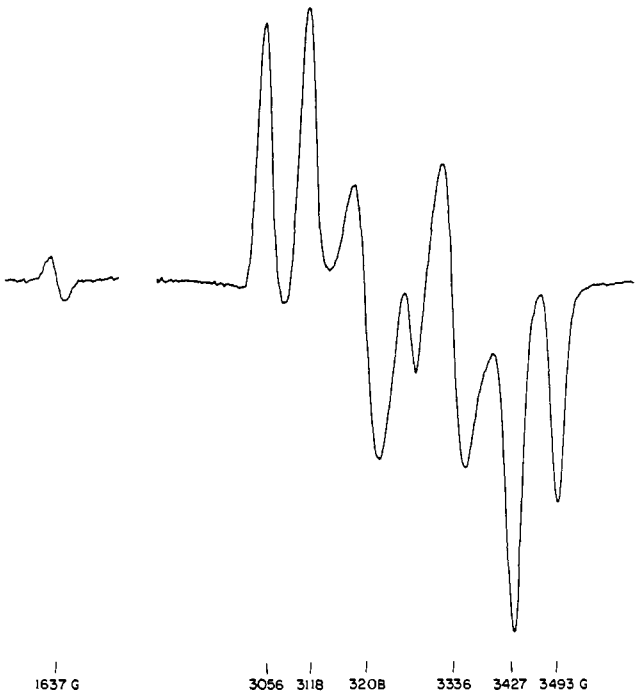

Figure 1. First-derivative EPR spectrum of ^{3}**1** ($|D/hc|$ = 0.0204 cm^{-1}, $|E/hc|$ = 0.0028 cm^{-1}) observed after 1 min of sensitized photolysis (1000-W Xe arc lamp; λ = 315–415 nm) of **2** in MTHF containing 0.3 M Ph_2CO at 5–6 K. The spectrum was recorded at 9.18 GHz and 0.002-mW microwave power.

of generation, the signal is unequivocally assigned to triplet biradical **1** (^{3}**1**) on the basis of its D value.

(57) Simulations were performed on an IBM PC/AT with a FORTRAN program obtained from E. F. Hilinski, which was originally written by J. M. McBride. The simulation uses the method of Kottis and Lefebvre.[58] See, also: Reference 59a. The program was adapted for use on the PC/AT (see Jain, R. Ph.D. Thesis, California Institute of Technology, 1987) and modified to incorporate isotropic hyperfine splitting.[47a]

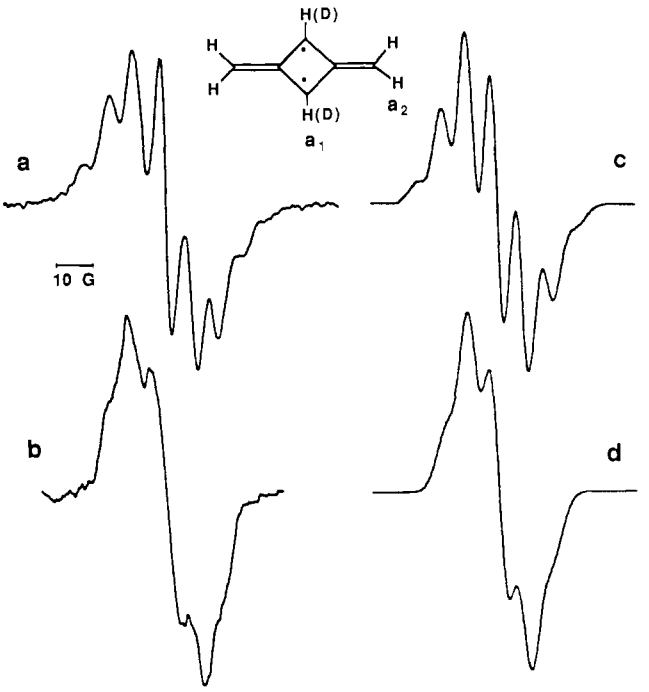

Figure 2. Hyperfine structure of the Δm_s = 2 transition. (a) The 1637-G signal of Figure 1 enhanced with 2.0-mW power and 3-G field modulation. (b) The analogous signal of **1**-d_2 (obtained under similar conditions of signal generation and measurement). (c, d) Spectra simulated by using isotropic proton coupling constants a_1 = 7.3 G and a_2 = 5.9 G and a 5.8-G line width.

The D value manifests itself in the width of the primary (Δm_s = 1) six-line region of a triplet EPR spectrum. This parameter is a gauge of the magnitude of the dipolar coupling between the unpaired spins, which lifts the degeneracy of the triplet sublevels even in the absence of an external magnetic field. The extent of this spin–spin interaction depends critically on the unpaired spin distribution and is therefore a sensitive probe of electronic structure. The D value of **1** is very much in accord with expectations based on related structures.[55] For example, it lies between values for the four-carbon π-system TMM ($|D/hc|$ = 0.0248 cm^{-1})[60] and the eight-carbon π-system m-xylylene ($|D/hc|$ = 0.011 cm^{-1}).[61] The E value is generally treated as a symmetry parameter only—a value of zero being a necessary but insufficient criterion for assigning the signal carrier an axially symmetric structure—and we attach no qualitative significance to the E value observed for **1**. Subsequent to our initial observation of **1**, corroborative evidence concerning the assignment was provided by Dowd and Paik, who independently generated a signal ascribed to **1** by sensitized photolysis of ketone **23**.[62]

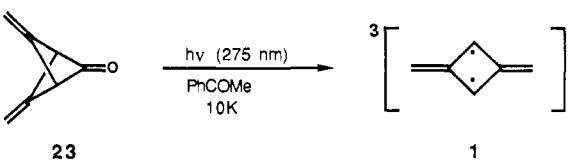

(58) Kottis, P.; Lefebvre, R. *J. Chem. Phys.* **1963**, *39*, 393–403; **1964**, *41*, 379–393.

(59) (a) Wasserman, E.; Snyder, L. C.; Yager, W. A. *J. Chem. Phys.* **1964**, *41*, 1763–1772. (b) deGroot, M. S.; van der Waals, J. H. *Physica* **1963**, *29*, 1128–1132. The transition intensity is much more power-dependent than the surrounding Δm_s = 1 lines. In addition, this central line vanishes reversibly on going to very low power or higher temperature and irreversibly upon photochemical destruction of the biradical (see below).

(60) (a) Dowd, P. *J. Am. Chem. Soc.* **1966**, *88*, 2587–2589. (b) Claesson, O.; Lund, A.; Gillbro, T.; Ichikawa, T.; Edlund, O.; Yoshida, H. *J. Chem. Phys.* **1980**, *72*, 1463–1470. (c) Yoshida, H.; Edlund, O. *Chem. Phys. Lett.* **1976**, *42*, 107–110. (d) Yamaguchi, T.; Irie, M.; Yoshida, H. *Chem. Lett.* **1973**, 975–978.

(61) Wright, B. B.; Platz, M. S. *J. Am. Chem. Soc.* **1983**, *105*, 628–630. Goodman, J. L.; Berson, J. A. *J. Am. Chem. Soc.* **1985**, *107*, 5409–5424; **1984**, *106*, 1867–1868.

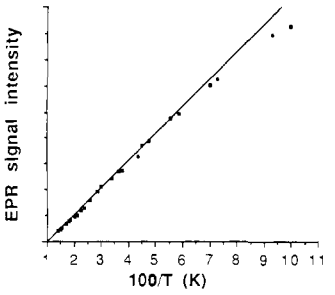

Figure 3. Curie law plot of the first-derivative EPR signal intensity of ^{3}**1** (in 1:1 EtOH/MeOH) as a function of temperature between 10 and 75 K.

The photochemical conversion of **2** to **1** is apparently quite efficient—the spectrum of Figure 1 was generated by only 1 min of sensitized photolysis. This spectrum is completely free of monoradical impurities; the central line near 3270 G is a double-quantum transition, so assigned on the basis of its strong microwave power dependence.[59] We have also obtained this triplet EPR signal upon photolysis of frozen solutions of **2** in a variety of solvents in addition to MTHF, including Et_2O, 3-methylpentane (3-MP), CH_2Cl_2, acetone, Et_2O/EtOH (4:1), MeOH/EtOH (1:1), and toluene-d_8/3-MP (7:1).

Proton Hyperfine Splitting. Additional information concerning the unpaired electron distribution and further confirmation of the structure of triplet **1** are provided by the hyperfine splitting in the half-field ($\Delta m_s = 2$) transition.[55,63] Figure 2 shows both the seven-line pattern observed for **1** and the five-line pattern observed upon replacement of the ring hydrogens with deuteriums. Additionally, the second and fifth lines of the $\Delta m_s = 1$ region (3118 and 3427 G in Figure 1) display poorly resolved but discernable hyperfine structure[64a] with the same 6–7-G splitting observed in the half-field transition.

Electron–nuclear hyperfine as well as electron–electron dipolar interactions in immobilized species are, in general, anisotropic and thus dependent on orientation with respect to the applied magnetic field. It is, therefore, not immediately apparent that the observed structure of the $\Delta m_s = 2$ transition in our randomly oriented sample should be readily interpretable in terms of conventional hyperfine coupling constants. However, as discussed in detail elsewhere,[47a,55,64-66] for planar π-systems such as **1** the spacings seen in the $\Delta m_s = 2$ region of a powder spectrum very closely approximate those expected from purely isotropic hyperfine couplings. This is clearly demonstrated by comparison of single-crystal vs powder spectra of TMM.[60]

Given this analysis, the observed splitting of Figure 2 can be attributed by inspection to interaction with six protons that have comparable coupling constants in **1** and four in **1**-d_2. In fact, computer simulation[57] of these spectra reveals that the splitting constants a_1 and a_2 (Figure 2) although similar, are not identical. As shown in Figure 2c and d, we have obtained acceptable simulations of both experimental spectra by using splittings of a_1 = 7.3 G for two protons (7.3/6.5 for two deuterons) and a_2 = 5.9 G for four.[67a]

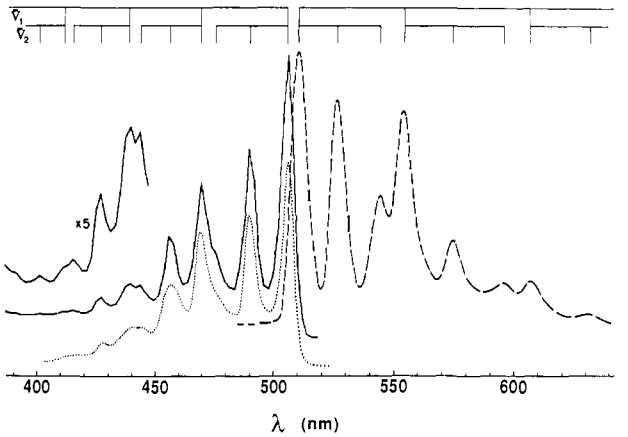

Figure 4. Absorption (—), fluorescence (- - -; λ_{ex} = 440 nm), and fluorescence excitation (···; λ_{em} = 550 nm) spectra of ^{3}**1** in MTHF at 77 K. λ_{max} = 506 and 510 nm for absorption and emission, respectively.

We note that the hyperfine structure observed is consistent only with the planar geometry for **1**. Rotation of the terminal methylene groups produces **1p** or **1pp**. The observed removal of the

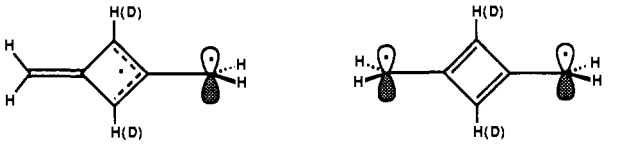

1p **1pp**

larger (7.3-G) splitting by deuteration at the methine positions obviates further consideration of **1pp**. With regard to **1p** we note that, to first order, the methylenecyclobutenyl moiety has spin density only at the ring methine positions. Removal of the larger splitting in going from **1** to **1**-d_2 is consistent with this idea. However, the five-line pattern observed for **1**-d_2 (Figure 2b) requires comparable spin densities on both methylenes, which is quite incompatible with structure **1p**.

Curie Plot. Figure 3 shows the variation in EPR signal intensity with reciprocal temperature. The data plotted were obtained upon first increasing then decreasing the temperature to demonstrate that the intensity change is reversible. Aside from the small deviation from linearity at the low-temperature end of the plot, which we attribute to saturation of the signal, the intensity adheres to the Curie law between 15 and 75 K. This indicates that the triplet is the ground state of **1** or that the singlet and triplet are nearly degenerate.[64c] In light of theoretical arguments presented above, we consider the first interpretation to be much more likely.

Electronic Spectroscopy

During our initial EPR experiments, we realized that the triplet biradical is quite photosensitive, being irreversibly destroyed by visible light. A simple filter-shuffling experiment established that light of $\lambda < 515$ nm was responsible for destroying the biradical, suggesting that triplet **1** has a strong electronic transition near 500 nm.

Indeed, when a sample of **2** in MTHF is irradiated with UV light, an intense yellow-orange color appears. In addition, the sample displays a bright, short-lived, green emission which is readily observable when the sample is placed in the UV–vis spectrophotometer beam. Figure 4 shows the absorption, emission, and excitation spectra of the colored species, obtained at 77 K.[14b] The correspondence between the absorption and excitation spectra formally demonstrates that the same species is responsible for both the absorption and emission observed.

Assignment of the Spectra to ^{3}1. We have compelling evidence that the absorption and emission spectra of Figure 4 are those of ^{3}**1**. That these spectra arise from **1** (i.e., are not due to an impurity or byproduct) is demonstrated by the coincident formation of the EPR and absorption spectra and their loss upon bleaching the sample with visible light. In addition, both the EPR

(62) Dowd, P.; Paik, Y. H. *J. Am. Chem. Soc.* **1986**, *108*, 2788–2790.

(63) For a general discussion of $\Delta m_s = 2$ hyperfine, see: Grivet, J.-Ph. *Mol. Phys.* **1970**, *19*, 389–398. See also: references 47a, 55, and 59a.

(64) Snyder, G. J. Ph.D. Thesis, California Institute of Technology, 1988; (a) p 55; (b) pp 140–141; (c) p 144; (d) pp 86–89.

(65) Sternlicht, H. *J. Chem. Phys.* **1960**, *33*, 1128–1132. See also: Lefebvre, R. *J. Chem. Phys.* **1960**, *33*, 1826–1829.

(66) Jain, R.; McElwee-White, L.; Dougherty, D. A. *J. Am. Chem. Soc.* **1988**, *110*, 552–560.

(67) (a) We place conservative error limits of ±0.6 G on a_1 and ±0.4 G on a_2. (The ratio of the coupling constants, a_1/a_2 = 1.24 ± 0.1.) (b) The absolute error limits on the spin densities are thus ±0.05 on ρ_1 and ±0.03 on ρ_2, and the ratio of spin densities is 1.15 ± 0.1. It is apparent from simulations that this ratio is different from 1.0 and substantially different from the Hückel ratio of 1.5. For a more detailed discussion, see: Reference 64b.

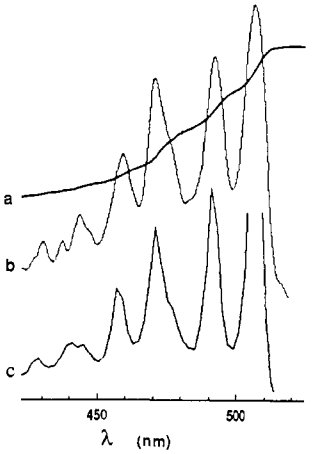

Figure 5. Photochemical action spectrum. (a) EPR signal intensity of **1** in MTHF at 4 K, monitored at the low-field *y* transition (3073 G; 9.27 GHz), vs irradiation wavelength. Scan is from right to left as presented and represents decay of approximately 65% of the original signal. (b) The function $\epsilon(\lambda) = (-dS/dt)(K/SI_0(\lambda))$ (see text), obtained from curve a by smoothing and numerical differentiation. (c) The 77 K absorption spectrum of Figure 4.

and absorption spectra decay very slowly ($t_{1/2}$ = ca. 30 h) at 77 K in MTHF.[68] The decay is nonexponential due to a distribution of matrix sites, which produces a distribution of rate constants. This kinetic behavior can often be treated by plotting ln I vs $t^{1/2}$,[69] and such plots of the EPR and absorption intensities were linear and provided the same "most probable" rate constant.[69]

The above observations are consistent with our assignment; however, they do not rule out the possibility that the optical spectra result not from ^{3}**1** but rather from a species in rapid equilibrium with ^{3}**1**, singlet **1** (^{1}**1**) being the obvious candidate. The optical spectra were recorded at 77 K, which would allow significant population of a higher lying singlet even if the S–T gap were on the order of a few kcalories per mole. The photodestruction of the EPR signal was observed at 4 K. However, this could simply indicate that ^{3}**1** also has an absorption near 500 nm that is overwhelmed by the singlet absorption at 77 K. Ideally, one would resolve this conflict by simply measuring the absorption spectrum at 4 K, but we could not easily conduct such an experiment.

We have, however, been able to measure an effective absorption spectrum and at the same time explicitly link the optical spectra of Figure 4 and the EPR spectrum *at 4 K*. The well-defined vibronic structure of the absorption envelope and the efficient photochemical destruction of ^{3}**1** suggested that, if the 77 K absorption spectrum persisted at 4 K, monochromatic irradiation of ^{3}**1** at an absorption peak would produce detectably faster decay of the EPR signal than irradiation between peaks. An implementation of this experiment is shown in Figure 5a. Scanning from higher to lower irradiation wavelength (right to left as shown) at a constant rate with a monochrometer, the EPR signal intensity falls off rapidly at precisely the wavelengths of the vibronic peaks of the 77 K absorption spectrum. The signal intensity curve can be converted to an ϵ vs λ spectrum in a straightforward manner.

The rate of photochemical loss of ^{3}**1**, whose concentration, c_T, is proportional to the EPR signal intensity, S, is given by

$$-\frac{dS}{dt} = KI_0(\lambda)A(\lambda)\Phi_r$$

where K is a proportionality constant. The quantum yield for reaction from the excited state, Φ_r, is assumed to be wavelength independent (vibrational relaxation is rapid), while I_0, the incident light intensity, varies slightly with λ. Expressing absorbance as $\epsilon c_T l$ and gathering constants, we have

$$-\frac{dS}{dt} = K'I_0(\lambda)c_T\epsilon(\lambda)$$

Again relating c_T to signal intensity, we can express ϵ as

$$\epsilon(\lambda) = K''\left(-\frac{dS}{dt}\right)\left(\frac{1}{SI_0(\lambda)}\right)$$

The incident light intensity, $I_0(\lambda)$, can be approximated as the Xe arc lamp output spectrum, which is easily measured. Finally, since the irradiation wavelength was changed at a constant rate, the λ axis is also a time axis. Therefore, simply differentiating the signal intensity function (Figure 5a) with respect to λ and dividing by incident light and signal intensities provides a curve proportional to $\epsilon(\lambda)$ vs λ for the EPR signal carrier.

This curve is presented as Figure 5b along with the 77 K absorption spectrum on the same scale for comparison (Figure 5c). The agreement between the two is apparent. It is worth emphasizing that this EPR-detected photochemical destruction profile, or "photochemical action spectrum", provides an *explicit* link between the 77 K absorption spectrum of Figure 4 and the 4 K EPR signal of Figure 1. This connection is quite analogous to that between absorption and emission spectra provided by an excitation spectrum; the action spectrum simply monitors decay rate rather than emission intensity. Again, this spectrum could arise from ^{1}**1** if the S–T gap is so small that there is significant S population at 4 K, and again we reject this interpretation on the basis of the arguments presented above. We accordingly conclude that the optical spectra of Figure 4 belong to the EPR signal carrier ^{3}**1**.

The Nature of the Electronic Transition. Having established the identity of the species responsible for the electronic spectra, we can determine the oscillator strength of the transition by directly relating the intensity of the absorption spectrum to the concentration of ^{3}**1**. Thus, a sample of **2** in an MTHF glass at 77 K was irradiated so as to produce a uniform distribution of biradical with an absorbance of ca. 0.5 at 506 nm (path length 0.35 cm). The concentration of ^{3}**1** in the sample was then found to be ca. 2×10^{-4} M by comparison of the intensity of its double-integrated EPR spectrum with that of a standard free-radical sample. Multiple measurements then provided an ϵ(506) of 7200 (±2000) M^{-1} cm^{-1}. Using this value, numerical integration of the absorption spectrum allowed calculation of the transition oscillator strength[70] as f = 0.022 (±0.006). The strength of the absorption indicates that the transition is spin-allowed,[71] and therefore that the emission of Figure 4 is a fluorescence.

The absorption spectrum is virtually independent of solvent [C_7D_8/3-MP (5:1), MTHF, Et_2O, Et_2O/EtOH, MeOH/EtOH (1:1)]; the only significant solvent effect we have observed is a ca. 1.5-nm blue-shift on going from MTHF (Figure 4) to 1:1 MeOH/EtOH. The virtual absence of a solvent effect implies a minimal change in polarity accompanying the excitation, as one might expect for a transition confined to the π-system of planar ^{3}**1**.

The electronic transition is coupled to two independent vibrational modes, producing vibronic spacings $\bar{\nu}_1$ and $\bar{\nu}_2$ (Figure 4). The highly resolved vibrational structure in these spectra is quite consistent with the rigid structure of the biradical. The striking mirror-image relationship between the two vibronic envelopes, the prominence of the 0–0 bands, and the small (150-cm^{-1}) Stokes' shift imply nearly identical geometries for the ground and excited states. Spacing $\bar{\nu}_1$ differs slightly in the absorption and emission spectra, with values of 1520 and 1570 cm^{-1} for the excited and ground states, respectively. The value of $\bar{\nu}_2$ is measured as ca. 620 cm^{-1} in each. The absorption spectrum of **1**-d_2 is experi-

(68) Slow decay is observed in a variety of solvents, but interestingly, the EPR signal intensity does not decrease perceptibly at 77 K in 1:1 EtOH/MeOH.

(69) The most probable rate constant in the distribution, k_0, is given by $k_0 = c^2/6$, where c is the slope of the plot: Doba, T.; Ingold, K. U.; Siebrand, W. *Chem. Phys. Lett.* **1984**, *103*, 339–342. Doba, T.; Ingold, K. U.; Siebrand, W.; Wildman, T. A. *J. Phys. Chem.* **1984**, *88*, 3165–3167. The half-life is then given by $t_{1/2} = (\ln 2)^2/6k_0$.

(70) Turro, N. J. *Modern Molecular Photochemistry*, Benjamin/Cummings: Menlo Park, CA, 1978; p 87.

(71) For example, see: Reference 70, Chapter 5, pp 76–152.

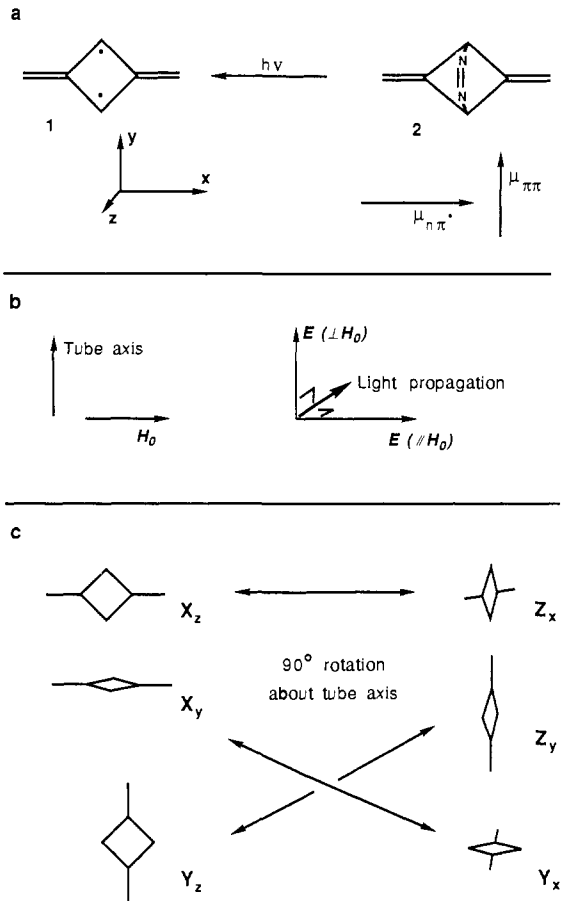

Figure 6. (a) The molecular axes defined for biradical **1** and the n_-,π^* transition dipole moment vector of the azo group of **2**. (b) The orientations of the sample tube, static magnetic field, and electric vector of the incident light. (c) The six principal canonical orientations of biradical **1**. The orientations are denoted by the molecular axis aligned with $\mathbf{H}_0$, with subscripts referring to the axis aligned with the incident light beam. Orientations interconverted by a 90° rotation of the sample tube are connected by arrows (rotation interchanges the primary and subscripted axis designations).

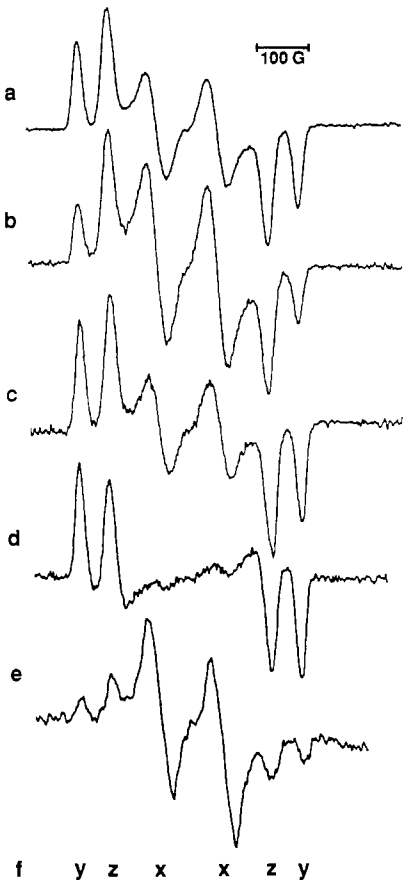

Figure 7. Magnetophotoselection experiments performed by irradiating a 77 K sample of **2** in an MTHF glass with linearly polarized 333 (±4) nm light. (a) The first-derivative EPR signal of an isotropic sample of triplet **1** for comparison. (b) The spectrum observed upon irradiation with $\mathbf{E}\|\mathbf{H}_0$. (c) The spectrum afforded by rotating the sample in (b) 90° about the tube axis. (d) The signal produced by photolyzing an isotropic sample of the biradical (Figure 7a) with 490-nm light having $\mathbf{E}\|\mathbf{H}_0$. (e) The signal observed after photolyzing an isotropic sample of **1** with *unpolarized* visible light ($\lambda > 485$ nm) and then rotating the sample 90° about the tube axis. (f) Assignment of the transitions in terms of the molecular axes as defined in Figure 6a.

mentally indistinguishable from that of **1**, consistent with the expectation that the active vibrations do not involve the methine C–H bonds. Further information on the nature of the electronic spectra could be obtained from magnetophotoselection experiments, as described in the next section.

Assignment of the Principal Axes and Transition Moment

Magnetophotoselection. Additional information concerning the electronic structure of ^{3}**1** is potentially available if the three pairs of $\Delta m_s = 1$ EPR transitions can be assigned to the structural axes of the biradical. We have made such an assignment by (in part) the technique of magnetophotoselection,[72] In addition, we have used magnetophotoselection to establish the polarization of the optical transition in **1**.

The Zero-Field Triplet Sublevels. Biradical **1** is of sufficiently high symmetry that the principal axes of the spin–spin dipolar coupling tensor are coincident with the symmetry axes of the molecular frame, as defined in Figure 6a. In a rigid, random ensemble of triplet species the EPR resonant field strength for a specific orientation depends on $3\cos^2\theta - 1$, where θ represents the angle between the applied magnetic field direction, $\mathbf{H}_0$, and one of the principal elements of the dipolar coupling tensor.[54] Due to this angular dependence, the EPR spectra of such samples are dominated by those species that have one of their principal axes aligned with or *nearly* aligned with $\mathbf{H}_0$. Thus, each pair of lines corresponds to a group of orientations with a principal dipolar coupling axis—and for ^{3}**1** also a molecular symmetry axis—approximately aligned with $\mathbf{H}_0$.

In order to relate the EPR transitions to the molecular axes, it is necessary to study the EPR spectra of triplets in known orientations. Irradiation of diazene **2** at 333 nm excites the n_-,π^* transition of the azo chromophore, which is polarized in the direction of the nitrogen p-orbital axes,[73] as shown in Figure 6a. Barring some contortionistic nitrogen extrusion mechanism, the preferred orientation of the biradical formed is then expected to be that in which its x axis, as defined in Figure 6a, lies in the direction of $\mu_{n\pi^*}$ of **2**.

An isotropic distribution of **1** in a rigid medium can be conveniently thought of in terms of the six principal orientations[74] shown in Figure 6c. The orientations are labeled according to the molecular axis of **1** aligned with $\mathbf{H}_0$ (horizontal in the laboratory frame—see Figure 6b), with subscripts referring to the biradical axis perpendicular to the page.

(72) (a) Chisholm, W. P.; Yu, H. L.; Murugesan, R.; Weissman, S. I.; Hilinski, E. F.; Berson, J. A. *J. Am. Chem. Soc.* **1984**, *106*, 4419–4423. (b) Chisholm, W. P.; Weissman, S. I.; Burnett, M. N.; Pagni, R. M. *J. Am. Chem. Soc.* **1980**, *102*, 7103–7104. (c) Kottis, P.; Lefebvre, R. *J. Chem. Phys.* **1964**, *41*, 3660–3661. Lhoste, J.-M.; Haug, A.; Ptak, M. *J. Chem. Phys.* **1966**, *44*, 648–654; 654–657. (d) El-Sayed, M. A.; Siegel, S. *J. Chem. Phys.* **1966**, *44*, 1416–1423.

(73) (a) Suzuki, H. *Electronic Absorption Spectra and Geometry of Organic Molecules*; Academic: New York, 1967; pp 499–501. (b) Rau, H. *Angew. Chem., Int. Ed. Engl.* **1973**, *12*, 224–235. Mirbach, M. J.; Liu, K. C.; Mirbach, M. F.; Cherry, W. R.; Turro, N. J.; Engel, P. S. *J. Am. Chem. Soc.* **1978**, *100*, 5122–5129.

(74) Albrecht, A. C. *J. Mol. Spectrosc.* **1961**, *6*, 84–108.

Figure 7a shows the EPR spectrum of an isotropic distribution of ^{3}**1** generated by photolyzing a sample of **2** in an MTHF glass at 77 K. When this photolysis is conducted using a polarizer to select UV light with the electric field vector, **E** (not to be confused with the zfs parameter E), parallel to $\mathbf{H}_0$ ($\mathbf{E}\|\mathbf{H}_0$; see Figure 6b), biradical orientations $\mathbf{X}_y$ and $\mathbf{X}_z$ (Figure 6c) should be formed preferentially, and the EPR transitions corresponding to the x axis should be the only ones observed. Figure 7b shows the result of such an experiment. The two inner transitions are clearly enhanced relative to the isotropic spectrum. Rotation 90° around the tube axis causes the conversions $\mathbf{X}_y \rightarrow \mathbf{Y}_x$ and $\mathbf{X}_z \rightarrow \mathbf{Z}_x$ (rotation interchanges the subscripted and primary labels). As shown in Figure 7c such a rotation, which places the photochemical imprint of **E** perpendicular to $\mathbf{H}_0$, does lead to substantially weakened x lines relative to y and z. As expected, an identical spectrum is generated by photolysis with **E** perpendicular to $\mathbf{H}_0$ ($\mathbf{E}\perp\mathbf{H}_0$). We therefore assign the inner pair of transitions (3208 and 3336 G in Figure 1) to the x axis of **1**. Of course, owing to some scattering and reflection of the UV light, the polarization is not perfect, and all six transitions are present in both spectra.[75]

Additionally, our observation of discernable hyperfine splitting with the isotropic pattern in the second and fifth $\Delta m_s = 1$ peaks, but none in the outer pair (see above), allows us to assign the former pair to the biradical z axis and the latter to the y (Figure 7f). For ^{3}**1** the principal axes of the hyperfine coupling tensors for the two types of protons are coincident only in the z direction. Moreover, the anisotropic tensor element in this direction is very nearly zero, effectively leaving only the isotropic contribution. Therefore, only the z transition should display the same isotropic splitting pattern as is observed in the $\Delta m_s = 2$ transition (the z transitions of a randomly oriented sample of TMM also display the isotropic splitting pattern for this reason[60c,d]).

Finally, we have established that the D value for ^{3}**1** is negative. This determination derives from the intensity differences between the low-field and high-field members of each pair of $\Delta m_s = 1$ transitions at very low temperature.[76] One member of each pair arises from an $m_s = -1 \rightarrow 0$ transition, the other an $m_s = 0 \rightarrow 1$ transition.[54] At sufficiently low temperature the Boltzmann populations of the three states are such that the former transition becomes significantly more probable than the latter. On going from 77 K (Figure 7a) to near 4 K (Figure 1) the low-field y peak and the high-field z and x peaks are clearly enhanced. This pattern implies that $D < 0$, the final piece of information necessary to establish the relative energies of the zero-field eigenstates of ^{3}**1** in terms of the molecular symmetry axes. These are presented below, along with their relationships to the zero-field splitting parameters.

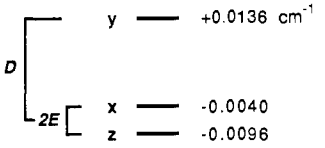

The Electronic Transition Dipole Moment. Having assigned the three pairs of $\Delta m_s = 1$ EPR transitions to the molecular axes of ^{3}**1**, we can exploit the photochemical lability of the biradical to determine its electronic transition moment. When an isotropic sample of ^{3}**1** (Figure 7a) in a good optical quality MTHF glass at 77 K is irradiated with visible light, polarized such that $\mathbf{E}\|\mathbf{H}_0$, the spectrum of Figure 7d is observed.[77] The virtual absence of the x transitions implies that biradicals whose x axes had been aligned with $\mathbf{H}_0$, namely, orientations $\mathbf{X}_z$ and $\mathbf{X}_y$ (Figure 6c), were selectively photolyzed, and accordingly that the electronic transition is x-polarized.

(75) There is also a secondary intensity variation evident in the y and z lines, especially in Figure 7c. Possible origins of this effect are discussed elsewhere.[64d] A similar effect was seen, but not discussed, in ref 72a.

(76) Hornig, A. W.; Hyde, J. S. *Mol. Phys.* **1963**, *6*, 33–41.

(77) Rotation of the sample tube by 90° transforms the **X**-depleted assembly (see Figure 6) into one with primary orientations $\mathbf{X}_z$, $\mathbf{X}_y$, $\mathbf{Y}_z$, and $\mathbf{Z}_y$. As expected, such a rotation then transforms the spectrum of Figure 7d into one whose x transitions are roughly twice as intense as their neighbors.

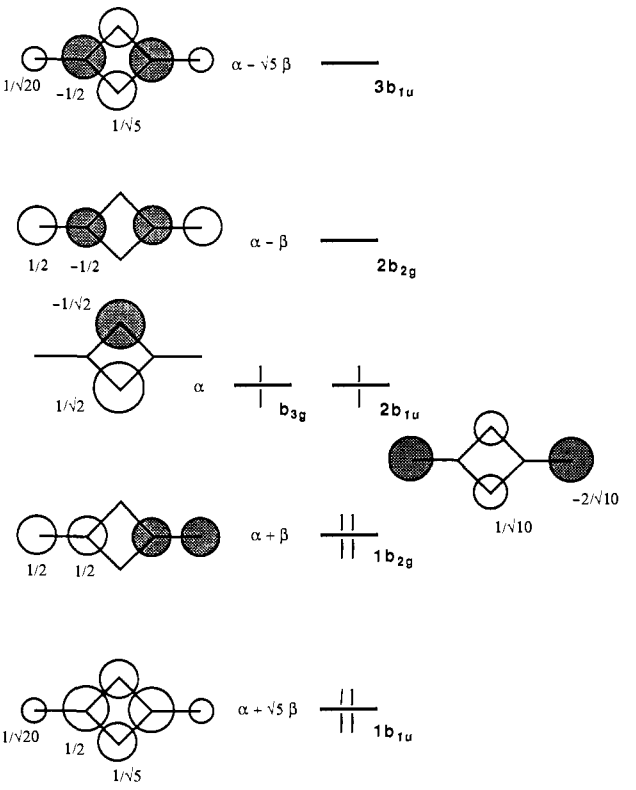

Figure 8. Hückel molecular orbitals of **1**.

The spectrum of Figure 7d results from a significantly more anisotropic distribution of triplets than that generated by polarized UV light photolysis of **2** (Figure 7b,c). This is most likely a result of two factors: (1) scattering and the resulting depolarization is more efficient for shorter wavelength light,[78] and (2) the nature of the present experiment, a competitive *destruction* of the different orientations (by polarized vs depolarized light) should produce an inherently more anisotropic distribution than the previous competitive *formation* experiment of Figure 7b and c.

We have been able to assign the transition moment by a second experiment that is conceptually less obvious but perhaps more interesting than the first. Ignoring depolarization effects, simple photolysis of an isotropic distribution of **1** with unpolarized light should not destroy all orientations equally.[74] This is, of course, because the **E** vector of the incident light is orthogonal to the direction of its propagation. Consequently, photolysis of an isotropic sample of ^{3}**1** with unpolarized visible light should destroy all of the biradical orientations except those whose electronic transition dipole moments lie in the direction of the light propagation. Rotating the sample tube 90° then points this molecular axis of the remaining biradicals along $\mathbf{H}_0$ (see Figure 6b,c) and the transition moment is simply read off the EPR spectrum.

Indeed, irradiation of an isotropic sample of **1** in MTHF with low-intensity light of $\lambda > 485$ nm provides a spectrum similar to that of Figure 7d. This presumably results from orientations $\mathbf{Z}_x$ and $\mathbf{Y}_x$ (Figure 6c) having been spared from photolysis. Rotation of the sample tube transforms these to $\mathbf{X}_z$ and $\mathbf{X}_y$, and the spectrum of Figure 7e is obtained. This confirms that the visible electronic transition of triplet **1** is polarized along the biradical x axis. Given that the transition is symmetry-allowed ($f = 0.022$) and that the ground state of biradical **1** is $^3B_{2u}$ (Figure 8), our finding that the transition is x-polarized implies that the excited-state symmetry must be $^3B_{1g}$.

Of course, similar anisotropy should arise from direct photolysis of **2** (with unpolarized light) to generate **1**, although the effect should be smaller for the reasons discussed above. The effect is, in fact, observable (see Experimental Section). Thus, the isotropic

(78) The intensity of the scattered light depends on λ^{-4}: Berne, B. J.; Pecora, R. *Dynamic Light Scattering*; Wiley: New York, 1976; p 27.

spectrum of Figure 7a was obtained by rotating the sample tube 90° halfway through the photolysis. True isotropy would require a third photolysis driection—along the tube axis. However, depolarization effects have likely rendered this third photolysis superfluous, and we consider the spectrum of Figure 7a to be essentially isotropic.

Discussion

Concerning the Singlet–Triplet Splitting. Triplet biradical **1** has proven to be quite amenable to spectroscopic study, in some respects exceptionally so. We have been able to observe and study ^{3}**1** at temperatures as low as 4 K, and all our experiments are completely consistent with the theoretical predictions of a decided triplet preference for the biradical. Unfortunately we cannot address the magnitude of this preference, even to the extent of placing a lower limit on the S–T gap. One might expect that a Curie plot would provide such information if the singlet were not far above the triplet in energy; however, these plots are extremely insensitive to termal population of even a very low lying singlet.[64c] Additionally, the electronic spectroscopy could be quite informative in this regard if one were able to observe specta attributable to ^{1}**1**, but again only spectra arising from the triplet ground state were observed. Having found no evidence to contradict the theoretical predictions, we conclude that the S–T gap for **1** is *substantial*, i.e., several kilocalories per mole.

Spin Densities and Spin Polarization. The determination of the relative spin densities at the ring and exocyclic positions of **1** is especially important from a theoretical standpoint. In particular, an adequate treatment of spin polarization[79a] is critical to the calculation of the relative energies of biradical electronic states as well as their geometries.[79a,80] Spin polarization generally makes the spin densities at the radical centers of triplet biradicals larger than those predicted on the basis of the NBMO coefficients alone. This effect operates by providing correlation of electrons in doubly occupied MOs with those in the NBMOs.

In TMM such an increase in spin density at the methylene positions is apparent from the proton hyperfine splitting observed.[79b] Similarly, the hyperfine splitting for ^{3}**1** reveals the influence of spin polarization. The measured splitting constants, a_1 = 7.3 G and a_2 = 5.9 G can be related to the spin densities, ρ_1 and ρ_2, at the ring and methylene carbons, respectively, by the relationship[81,82]

$$a_i = \tfrac{1}{2}Q\rho_i$$

where Q is a proportionality constant determined from studies of free radicals.[85] Thus, for **1**, ρ_1 = 0.56 and ρ_2 = 0.48.[67b] Given the difficulty in the measurement and the assumption that the observed splitting constants represent precisely the isotropic values (as well as some amount of uncertainty in the Q values used), our determination of ρ_1 and ρ_2 is certainly less accurate than similar measurements made from single-crystal spectra[60b,86] (or from fluid-media studies on monoradicals). We do, however, place

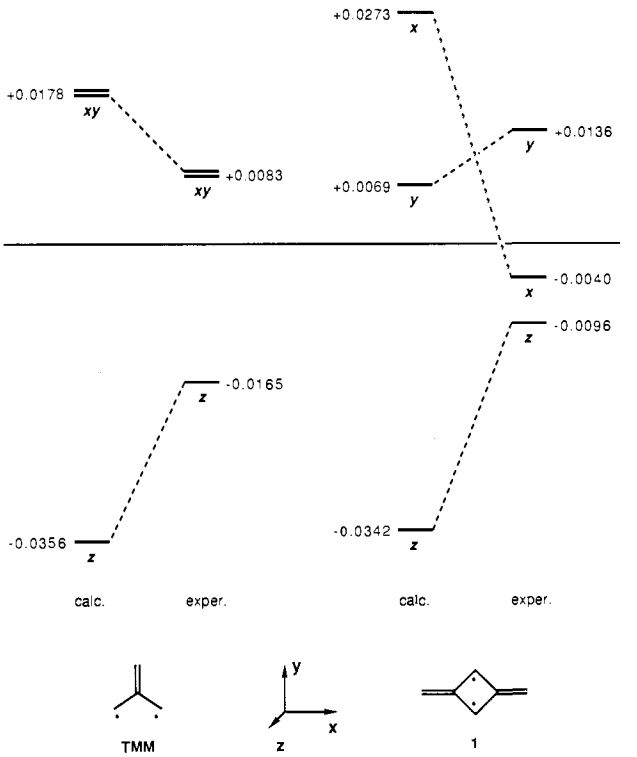

Figure 9. Calculated and experimental zero-field triplet sublevels for TMM[60] and **1** (see text) (in units of cm^{-1}).

significance on the relative spin densities derived from the measured splittings. Specifically, spectral simulation reveals that the *ratio* of spin densities, ρ_1/ρ_2, is 1.15 ± 0.1.[67b]

Figure 8 shows the Hückel MOs of **1**. The AO coefficients of the NBMOs derived at this level of theory imply spin densities ρ_1 = 0.6 and ρ_2 = 0.4 (ρ_1/ρ_2 = 1.5) at the ring and exocyclic radical centers, respectively. It is noteworthy that the higher spin density at the ring carbons is a result of the symmetry properties of the NBMOs. This is because the antisymmetric orbital, b_{3g}, is confined by symmetry to the ring carbons, while its counterpart, $2b_{1u}$, occupies both ring and methylene positions. Our experimental spin densities are qualitatively consistent with this expectation.

However, the experimental numbers indicate that the ratio ρ_1/ρ_2 is much smaller than anticipated. This finding is consistent with qualitative spin polarization arguments. Computationally, spin polarization can be treated by augmenting a single-determinant (RHF) wave function with configurations that involve one-electron excitations from a bonding MO to an antibonding MO having the proper phase relationships.[79] In ^{3}**1**, the dominant correlation effect involves $1b_{2g} \rightarrow 2b_{2g}$ (Figure 8) excitations. Because $1b_{2g}$ has a node at the ring methines, spin polarization of its electron pair can increase the total spin density only at the exocyclic methylene carbons. The experimental results support this argument, as do the results of UHF calculations, which find ρ_1 and ρ_2 to be 0.70 and 0.58, respectively (ρ_1/ρ_2 = 1.21).[87]

Zero-Field Splitting. Additional information concerning the electronic structure of triplet **1** is provided by our assignment of the zero-field triplet eigenstates to the symmetry axes of the biradical. However, attempting to relate this information in a qualitative sense to electronic structural features of **1**—or, more generally, of any biradical with extensively delocalized spins—is impractical. One reason for this is that spin polarization (see above) plays a major role in determining the magnitude of the dipolar coupling in delocalized biradicals.[83] For example, simple Hückel or RHF[83] treatments provide a D value for TMM that is approximately twice the experimental value. Higher level

(79) (a) For a general discussion of spin polarization, see: Reference 12, pp 15–17; (b) pp 25–27.

(80) Borden, W. T.; Davidson, E. R.; Feller, D. *Tetrahedron* **1982**, *38*, 737–739.

(81) The factor of $^1/_2$ is included for triplets when the exchange interaction is much larger than $|A_0|$. ($a = hA_0/g\beta$): Reitz, D. C.; Weissman, S. I. *J. Chem. Phys.* **1960**, *33*, 700–704. See also: Reference 54, pp 250–255.

(82) Use of the more accurate relationship[83,84a]

$$a_i = \tfrac{1}{2}(Q_i\rho_i + Q_j\rho_j)$$

where the second term refers to the negative spin density on the adjacent carbon (j) with Q_j = −1.9 G, does not significantly change the calculated spin densities.

(83) Feller, D.; Borden, W. T.; Davidson, E. R. *J. Chem. Phys.* **1981**, *74*, 2256–2259. See also: Reference 79b.

(84) (a) Gold, A. *J. Am. Chem. Soc.* **1969**, *91*, 4961–4963. (b) Gondo, Y.; Maki, A. H. *J. Chem. Phys.* **1969**, *50*, 3638–3639.

(85) We use Q = 24.4 and 26.2 G for CH_2 and CH centers, respectively. See: Reference 54, p 121.

(86) Dowd, P.; Gold, A.; Sachdev, K. *J. Am. Chem. Soc.* **1968**, *90*, 2715–2716.

(87) Hashimoto, K.; Fukutome, H. *Bull. Chem. Soc. Jpn.* **1981**, *54*, 3651–3658.

computational methods[83,84] demonstrate that an adequate treatment of spin polarization is essential for the calculation of D. Spin polarization also has a large effect on the spin–spin dipolar coupling tensor for ^{3}**1**, as is evident from a comparison of the experimental zero-field triplet sublevels with those calculated by using a Hückel wave function (Figure 9) and a previously described semiempirical scheme.[88] The calculated zero-field splitting patterns for TMM and **1** are quite similar, except that in TMM the x and y levels are degenerate by symmetry while in **1** these levels are strongly split. Experimentally, however, one finds that the D values for TMM and **1** have opposite signs. Moreover, for **1** the dominant interaction is in-plane (y), whereas for TMM the z axis carries the principal tensor element (Figure 9). While this seems to suggest that TMM is not a good reference point for **1**, these dissimilarities can be attributed simply to the different effects of spin polarization in the two biradicals.

As a result of spin polarization, the experimental zero-field splitting of TMM is reduced relative to the calculated (Hückel) splitting; however, the molecular symmetry requires that the energy level pattern remain the same. For **1** this is not the case. That is, spin polarization need not influence all three calculated energy levels in the same way. Thus, while the shift of the z level for **1** is quite similar to that of its counterpart in TMM, the x and y levels are perturbed in very different ways relative to their calculated positions (Figure 9). As it turns out, x drops close to z, so that the y element becomes determinant of D. In light of this result, some amount of caution would appear to be in order when using low-level wave functions to predict D values for delocalized biradicals.

Electronic Spectroscopy. The electronic transition energy of triplet **1** (506 nm; 56.5 kcal/mol) would, at first glance, appear exceptionally low for a molecule with a six-carbon π-system. However, **1** has a pair of NBMOs, which its fully covalent relatives lack. The transition occurs at a substantially longer wavelength than the transitions of benzene, fulvene, and 1,2-dimethylenecyclobutene,[89] but is not too different from the triplet–triplet transitions of several other non-Kekulē hydrocarbons.[7d,90-94]

The energy, oscillator strength, and polarization of the T–T transition of **1** are all in excellent agreement with the results of PPP–SCF–SCI calculations performed in our laboratory, which find a $^3B_{2u} \rightarrow {}^3B_{1g}$ transition at 501–504 nm (f = 0.01–0.02).[3d] These calculations indicate that the transition involves a combination of $1b_{2g} \rightarrow 2b_{1u}$ and $2b_{1u} \rightarrow 2b_{2g}$ (Figure 8) one-electron excitations.[3d] The relatively low oscillator strength results from the parity-forbidden nature of the transition.[3d,91]

Given these changes in orbital occupancy, we can tentatively assign the vibrations responsible for the double vibronic progression observed (Figure 4). Active vibrations generally correspond to the most important geometrical changes induced by the electronic transition.[95] It is reasonable to assume that the active vibrational modes for this π–π transition are confined to the carbon framework, since the C–H bonds lie in the nodal plane of the biradical's π-system. Our observation of identical absorption spectra for **1** and **1**-d_2 is consistent with this idea.

Referring to the MO diagram of Figure 8, we see that the excitation component $1b_{2g} \rightarrow 2b_{1u}$ depopulates an olefinic π-orbital, while the component $2b_{1u} \rightarrow 2b_{2g}$ populates the corresponding π^*-orbital. Thus, the excitation should lengthen the bonds to the exocyclic methylene groups, and the corresponding stretching vibration should be activated. We tentatively assign the larger vibrational frequency to such an A_g C–C "double-bond" stretching mode. Consistent with the weakening of these bonds in the excited state is the observation of a lower vibrational frequency in the absorption spectrum (1520 cm^{-1}) than in the fluorescence (1570 cm^{-1}). Additionally, because the transition involves an orbital that is bonding across the four-membered ring ($2b_{1u}$), one might expect a ring breathing-type mode to be activated. The set of A_g modes contains two such vibrations, and the 620-cm^{-1} spacing may well correspond to one of these.

Table I. Transmittance Data for Filter Combinations

no.	filters[a]	trans range,[b] nm	λ_{max}(trans), nm
1	WG-305/KG-5/UG-11	306 < λ < 386	355 (0.35)
2	no. 1 + 334 int[c]	326 < λ < 342	335 (0.08)
3	WG-305/KG-5/GG-495/NG-4	485 < λ < ca. 775[d]	550 (0.012)

[a] Obtained from Schott (3-mm thickness). [b] Cutoff values defined as 1% transmittance. [c] A 334-nm interference filter obtained from Oriel. [d] Cutoff values are defined as 0.1% transmittance for this combination.

Experimental Section[96]

General and Routine Instrumentation. Reagents were obtained commercially and used without purification unless otherwise noted. THF and MTHF were distilled from sodium benzophenone ketyl immediately before use. Other solvents used in synthetic procedures were reagent grade; those used for EPR and optical spectroscopic studies were Spectro grade or Gold Label. Glassware was base-washed (KOH/EtOH), especially prior to use for reactions involving bicyclobutanes. Flash chromatography[97] employed 230–400 mesh silica (EM Science, silica gel 60). Preparative-scale photolyses were conducted with a Pyrex-shrouded Hanovia 450-W medium-pressure Hg arc lamp in a water-jacketed immersion well. NMR spectra were recorded on JEOL FX-90Q or GX-400 spectrometers. ^{1}H and ^{13}C chemical shifts were determined relative to TMS by using the solvent signal as reference. Low-temperature NMR experiments were performed on the 400-MHz instrument and are discussed in more detail in the accompanying paper.[15] IR spectra were measured on a Perkin-Elmer 1310 spectrometer. Melting points were obtained with a Thomas-Hoover capillary melting point apparatus and are corrected. Combustion analyses and mass spectra were obtained by the Caltech analytical facility or the U.C. Riverside Mass Spectrometry Lab. EPR experiments, optical spectroscopy, and photolyses at 77 K were conducted by immersing the sample in a liquid N_2 filled quartz finger Dewar.

Spectroscopic Samples. Sample tubes for spectroscopic studies were Wilmad Glass 701-PQ 5-mm-o.d. medium-walled quartz tubes fitted via ground-glass joints to high vacuum stopcocks. Quartz tubes of 4-mm o.d. were used for EPR studies employing the Oxford cryostat (see below). Diazene samples were degassed by three freeze (liquid N_2)–pump–thaw (dry ice/acetone) cycles in subdued light on a vacuum line capable of maintaining ca. 10^{-3} mm and stored in the dark at 77 K or at −100 °C before use.

Photolysis. Cryogenic samples were irradiated with light from an Oriel 1000-W "ozone-free" Hg(Xe) or Xe arc lamp (operated at 950–980 W) mounted in a (Model No. 66023) housing equipped with an f/0.7 quartz lens assembly and water filter. The light was directed through a series of filter glasses in a water-filled chamber and focused onto the sample. The filter combinations used and their transmittance ranges are listed in Table I. Alternatively, the light was focused onto the entrance slit of an Oriel Model 77250 monochrometer equipped with a 200-nm-blaze holographic grating and calibrated against the Hg spectral lines. The Xe lamp output was measured accurately in the wavelength region of interest at 2–3-nm resolution by focusing the monochrometer output onto an Oriel Model 7104 spectrally neutral 5-mm-diameter thermopile detector.

EPR Experiments. Spectra were recorded on a Varian E-line Century Series X-band EPR spectrometer (TE_{102} cavity; $H_1 \perp H_0$) with an Oxford Instruments ESR-900 Continuous Flow Cryostat with liquid helium as the cryogen. The temperature of the helium stream was monitored continuously by an Au + 0.03% Fe vs chromel thermocouple located 1 cm below the EPR cavity and controlled by an Oxford Model 3120 temperature controller. The sample temperature was measured with a

(88) Rule, M.; Matlin, A. R.; Seeger, D. E.; Hilinski, E. F.; Dougherty, D. A.; Berson, J. A. *Tetrahedron* **1982**, *38*, 787–798.
(89) Blomquist, A. T.; Maitlis, P. M. *Proc. Chem. Soc., London* **1961**, 332. Meuche, D. *Helv. Chim. Acta* **1966**, *49*, 1278–1283.
(90) Turro, N. J.; Mirbach, M. H.; Harrit, N.; Berson, J. A.; Platz, M. S. *J. Am. Chem. Soc.* **1978**, *100*, 7653–7658. The source of the extremely weak 428-nm band is uncertain. See, for example: Reference 91.
(91) Gisin, M.; Wirz, J. *Helv. Chim. Acta* **1983**, *66*, 1556–1568.
(92) Roth, W. R.; Biermann, M.; Erker, G.; Jelich, K.; Gerhartz, W.; Görner, H. *Chem. Ber.* **1980**, *113*, 586–597.
(93) Migirdicyan, E.; Baudet, J. *J. Am. Chem. Soc.* **1975**, *97*, 7400–7404.
(94) Hasler, E.; Gassmann, E.; Wirz, J. *Helv. Chim. Acta* **1985**, *68*, 777–788. See also: Muller, J.-F.; Muller, D.; Dewey, H. J.; Michl, J. *J. Am. Chem. Soc.* **1978**, *100*, 1629–1630. Gisin, M.; Rommel, E.; Wirz, J.; Burnett, M. N.; Pagni, R. M. *J. Am. Chem. Soc.* **1979**, *101*, 2216–2218.
(95) Orchin, M.; Jaffē, H. H. *Symmetry, Orbitals, and Spectra*; Wiley: New York, 1971; p 227; ref 73a, p 86; ref 70, pp 92–93.
(96) Additional observations concerning many methodological aspects of this work can be found elsewhere.[64]
(97) Still, W. C.; Kahn, M.; Mitra, A. *J. Org. Chem.* **1978**, *43*, 2923–2925.

Lake Shore Cryotronics CGR-1-1000 carbon glass resistance sensor. Note that we previously reported[14a] a temperature of 10 K for the spectrum of Figure 1. Using this more accurate sensor, we have now determined that the actual temperature was 5-6 K. Essentially identical spectra are observed at 3.8 K.

UV-vis Absorption Spectroscopy. UV-vis spectra were recorded with a Hewlett-Packard 8451A diode array spectrophotometer with a deuterium source and equipped with an HP 85A microcomputer. Spectra of cryogenic samples in quartz tubes were recorded with air as the reference and with a 0.1-s measurement time. The nominal resolution of the instrument, dictated by the spacing of the diodes, is 2 nm; however, visual interpolation usually allowed reproducible resolution of the maxima for the sharp peaks of Figure 4 to better than 0.5 nm with at most ±0.5 nm uncertainty in their absolute positions.

***endo*,*endo*-2,4-Bis(hydroxymethyl)bicyclo[1.1.0]butane (6).** A variation of Christl's procedure was employed.[21a] A solution of benzvalene[98] (ca. 13.3 g, 0.171 mol) in 400 mL of ca. 3:1 ether/hexane (similar results have been obtained in ether only) was cooled to −78 °C. With magnetic stirring, a stream of O_3 in oxygen (Welsbach ozone generator set to deliver ca. 0.8 mmol of O_3 min^{-1}) was bubbled into the solution for 270 min (0.216 mol). The remaining ozone was purged with a stream of N_2, and the solvent was removed by rotary evaporation as the ozonide mixture warmed to room temperature. When the ozonide approached dryness,[99] ca. 50 mL of dry THF was added and rotary evaporation continued until ca. 20 mL of solvent remained. The yellow residue was dissolved in 400 mL of THF. A 5-L three-necked round-bottomed flask was fitted with a gas-tight mechanical stirrer, a thermometer, and a pressure-equalizing addition funnel topped with a gas inlet. The apparatus was dried with a flame under aspirator vacuum, pressurized with N_2, and cooled. Into the flask were placed 40.0 g (1.05 mol) of $LiAlH_4$ and 4 L of dry THF. Under a nitrogen atmosphere the slurry was cooled to −35 °C with a large-capacity CO_2/*i*-PrOH (−78 °C) bath, and the ozonide solution was placed in the addition funnel. With vigorous stirring this solution was added dropwise over 65 min while the slurry temperature was kept at −35 ± 1 °C. The mixture was then stirred at −35 °C for 60 min and at −31 °C for 30 min before cautious n,n,3n workup[100] below −30 °C. Thus, addition of the first 40 mL of water required 2.5 h; the following 40 mL of 3 N aqueous NaOH and 120 mL of H_2O were introduced over 30 min. The mixture was held at −35 to −40 °C for another hour, allowed to warm slowly, and stirred at room temperature overnight. The yellow mixture was dried over Na_2SO_4, the solids were removed by suction filtration and washed liberally with THF, and the solvent was removed under vacuum to afford 11.3 g of an orange syrup, which by ^1H NMR consisted of 9.9 g (51%) of **6**,[21] the remainder being hemiacetal[21] impurity. Typical (smaller scale) yields were ca. 55%. The product was carried forward without purification.

***endo*,*endo*-2,4-Bis[(*tert*-butyldimethylsiloxy)methyl]bicyclo[1.1.0]butane (7).** The crude diol **6** (9.9 g, 87 mmol) and 33.4 g (491 mmol) of imidazole were dissolved in 1 L of CH_2Cl_2, and 32.5 g (216 mmol) of *tert*-butyldimethylsilyl chloride was added.[101] The reaction was allowed to continue for 100 min at room temperature with magnetic stirring under a $CaCl_2$ drying tube. The CH_2Cl_2 solution was washed with water (4 × 300 mL) and brine (75 mL), dried (Na_2SO_4), and concentrated under vacuum to afford 35.5 g of clear, amber liquid. By ^1H NMR, the product consisted of ca. 25 g (85%) of **7**: ^1H NMR (400 MHz, $CDCl_3$) δ 3.55 (d, J = 6.1 Hz, 4 H, CH_2), 2.70 (m, 2 H, H-2,4), 1.56 (t, J = 3.8 Hz, 2 H, H-1,3), 0.86 (s, 18 H, *t*-Bu), 0.02 (s, 12 H, $SiMe_2$); ^{13}C NMR (22.6 MHz, $CDCl_3$) δ 65.0 (t, CH_2), 56.1 (d, C-2,4), 26.0 (q, *t*-Bu), 18.3 (s, *t*-Bu), 11.9 (d, C-1,3), −4.9 (q, $SiMe_2$). Again, we find it preferable to carry this material forward without purification; the major contaminant, *t*-$BuMe_2SiOH$, is conveniently removed at a later step.

(1α,2α,3β,4α)-1,3-Dibromo-2,4-bis(hydroxymethyl)cyclobutane. A cold (0 °C) solution of dibromide **9** in CCl_4 (ca. 150 mL) was prepared from benzvalene[98] (10.55 g, 135 mmol) by the procedure of Roth and Katz[25] and found to have a clean ^1H NMR spectrum identical with that reported.[25] This solution was immediately diluted with 600 mL of −60 °C CH_2Cl_2 and cooled to −78 °C. With magnetic stirring, a stream of O_3 in oxygen (ca. 0.8 mmol of O_3 min^{-1}) was bubbled into the solution for 190 min (152 mmol). The excess ozone was purged from the blue solution with N_2. The solvent was removed by rotary evaporation as the solution warmed, and the solid ozonide was dissolved in 450 mL of dry THF. In a dry 2-L three-necked round-bottomed flask bearing a gas-tight mechanical stirrer, a pressure-equalizing addition funnel, and an N_2 inlet-topped ice water condenser were placed 10.25 g (270 mmol) of $LiAlH_4$ and 1 L of anhydrous ether. The yellow ozonide solution was filtered and placed in the addition funnel, and the atmosphere in the apparatus was replaced with N_2. The solution was added dropwise with efficient stirring at such a rate as to maintain a brisk reflux (ca. 90 min), and heat was applied to sustain reflux for another 30 min. The reaction was quenched by the n,n,3n technique,[100] and the mixture was dried over Na_2SO_4 and filtered. The solvent was removed by rotary evaporation and the oily orange solid triturated with $CHCl_3$ and air-dried. Recrystallization of the off-white title compound (15.5 g, 42% from benzvalene) from acetone afforded a white solid: mp 138-139 °C; ^1H NMR (400 MHz, acetone-d_6) δ 4.97 (t, J = 7.3 Hz, 1 H, H-3[102]), 4.00 (t, J = 9.2 Hz, 1 H, H-1[102]), 3.77 (dd, J = 11.2, 8.3 Hz, 2 H, CH_2), 3.68 (dd, J = 11.2, 5.1 Hz, 2 H, CH_2), 2.95 (br m, 4 H, H-2,4 + OH (D_2O-exchangeable)); ^{13}C NMR (22.6 MHz, acetone-d_6) δ 62.2, 53.5, 52.1, 43.7; MS (EI) *m/e* (relative intensity) 272, 274, 276 (9, 18, 10, M^+), 241, 243, 245 (6, 9, 5; $M^+ - CH_3O$), 211, 213, 215 (15, 26, 13; $M^+ - C_2H_5O_2$), 193, 195 (39, 36; M^+ - Br), 175, 177 (98, 95; M^+ - Br, H_2O), 145, 147 (91, 100; M^+ - Br, H_2O, CH_2O). Anal. Calcd for $C_6H_{10}O_2Br_2$: C, 26.31; H, 3.68. Found: C, 26.74; H, 3.68.

(1α,2α,3β,4α)-1,3-Dibromo-2,4-bis[(*tert*-butyldimethylsiloxy)methyl]cyclobutane. To the dibromobis(hydroxymethyl)cyclobutane (1.00 g, 3.65 mmol), 1.25 g (18.4 mmol) of imidazole, and 200 mL of CH_2Cl_2 was added 1.20 g (7.96 mmol) of *tert*-butyldimethylsilyl chloride,[101] and the mixture was stirred magnetically under a $CaCl_2$ drying tube at room temperature for 20 h. The CH_2Cl_2 solution was washed with water (3 × 30 mL) and brine (10 mL), dried (Na_2SO_4), filtered through a pad of silica, and concentrated by rotary evaporation. Heating at 70 °C under vacuum for ca. 1 h to remove *t*-$BuMe_2SiOH$ afforded 1.65 g (90%) of the title compound as a colorless liquid: ^1H NMR (400 MHz, $CDCl_3$) δ 4.78 (t, J = 7.2 Hz, 1 H, H-3[102]), 3.86 (t, J = 9.2 Hz, 1 H, H-1[102]), 3.79 (dd, J = 10.5, 8.1 Hz, 2 H, CH_2), 3.74 (dd, J = 10.5, 5.4 Hz, 2 H, CH_2), 2.87 (m, 2 H, H-2,4), 0.88 (s, 18 H, *t*-Bu), 0.06 (s, 12 H, $SiMe_2$).

***exo*,*exo*-2,4-Bis[(*tert*-butyldimethylsiloxy)methyl]bicyclo[1.1.0]butane (8).** To a well-stirred solution of 5.05 g (10.1 mmol) of the dibromobis(siloxymethyl)cyclobutane in 350 mL of anhydrous ether at −78 °C under Ar, was added a 2.15 M solution of *t*-BuLi in pentane (11.8 mL, 25.4 mmol)[26] via syringe over 4 min. After 3.5 h the reaction was quenched by addition of 2.0 mL of water, and the mixture was allowed to warm to room temperature. The solution was washed with water (3 × 100 mL), dried (Na_2SO_4), and concentrated under vacuum to afford 3.46 g of a clear, colorless liquid. By ^1H NMR analysis this product is typically found to contain 50-65% of **8**: ^1H NMR (400 MHz, $CDCl_3$) δ 3.54 (d, J = 5.1 Hz, 4 H, CH_2), 1.40 (s, 2 H, H-1,3), 1.15 (t, J = 4.9 Hz, 2 H, H-2,4), 0.88 (s, 18 H, *t*-Bu), 0.04 (s, 12 H, $SiMe_2$); ^{13}C NMR (100 MHz, $CDCl_3$) δ 62.3 (t, CH_2), 43.1 (d, C-2,4), 26.0 (q, *t*-Bu), 18.4 (s, *t*-Bu), 3.3 (d, C-1,3), −5.3 (q, $SiMe_2$). In addition, ^1H NMR revealed the presence of ca. 2-3% of **7**.

4-Methyl-1,2,4-triazoline-3,5-dione (MTAD). 4-Methylurazole, prepared by literature methods[103] or obtained commercially, was oxidized with N_2O_4.[104] A typical reaction provided 35 g of MTAD as a red solid which was dried briefly under vacuum and used without further purification.

***exo*,*exo*-8,9-Bis[(*tert*-butyldimethylsiloxy)methyl]-4-methyl-2,4,6-triazatricyclo[5.1.1.$0^{2,6}$]nonane-3,5-dione (10).** The bicyclobutane (35.5 g of impure material containing 25 g of **7**, 73 mmol) was split into 11 portions. Each, in turn, was dissolved in 1 L of pentane, and ca. half of the requisite 4.25 g (37.6 mmol for each portion of **7**) of MTAD was added. The 450-W Hg arc lamp assembly was immersed in the solution, the vessel was connected to a source of N_2, and the mixture was stirred magnetically for ca. 5 min to saturate the solution with MTAD. With efficient stirring the mixture was irradiated for 40 min, the remaining MTAD was added, and the irradiation was continued for another 40 min. The solution was decanted, the sticky solid residue was washed with pentane, and the solvent was removed by rotary evaporation. The combined product, 86 g of a viscous yellow oil, was subjected to flash chromatography on a 10 cm × 5 in. silica column. Elution with 2.5 L of 4:1

(98) Katz, T. J.; Wang, E. J.; Acton, N. *J. Am. Chem. Soc.* **1971**, *93*, 3782-3783. Katz, T. J.; Roth, R. J.; Acton, N.; Carnahan, E. J. *Org. Synth.* **1973**, *53*, 157. The concentration of benzvalene was determined by NMR with mesitylene as an internal standard.

(99) Christl, M.; Brüntrup, G. *Chem. Ber.* **1974**, *107*, 3908-3914.

(100) Fieser, L. F.; Fieser, M. *Reagents for Organic Synthesis*; Wiley: New York, 1967; Vol. 1, p 584.

(101) Corey, E. J.; Venkateswarlu, A. *J. Am. Chem. Soc.* **1972**, *94*, 6190-6191.

(102) This assignment is made tentatively on the basis of chemical shifts[25] and coupling constants of protons in similar systems: Griesbaum, K.; Mach, H.; Hittich, R. *Chem. Ber.* **1982**, *115*, 1911-1921. Lemarie, B.; Braillon, B.; Lasne, M.-C.; Thuillier, A. *J. Chim. Phys.-Phys. Chim. Biol.* **1977**, *74*, 799-808.

(103) Cookson, R. C.; Gupte, S. S.; Stevens, I. D. R.; Watts, C. T. *Org. Synth.* **1971**, *51*, 121-127.

(104) Stickler, J. C.; Pirkle, W. H. *J. Org. Chem.* **1966**, *31*, 3444-3445.

(v/v) petroleum ether/ether provided 17.1 g of a pale yellow liquid. This was heated under vacuum (<1 mm) at 70–80 °C for 1 h to remove the residual *t*-BuMe$_2$SiOH. The resultant solid was flash chromatographed on a 10 cm × 5 in. silica column with 2 L of 19:1, 1.5 L of 5:1, and 1.5 L of 2:1 (v/v) petroleum ether (PE)/ether eluant to afford 12.4 g (37%) of **10** ($R_f \simeq 0.3$ in 4:1 PE/Et$_2$O) as a white solid: mp 91.5–94.0 °C; ^{1}H NMR (400 MHz, $CDCl_3$) δ 4.69 (t, $J_{1,8}$ = 1.8 Hz, 2 H, H-1,7), 3.35 (d, J = 6.6 Hz, 4 H, CH_2), 3.01 (s, 3 H, NCH_3), 2.42 (tt, J = 1.8, 6.5 Hz, 2 H, H-8,9), 0.84 (s, 18 H, *t*-Bu), −0.01 (s, 12 H, $SiMe_2$); ^{13}C NMR (22.6 MHz, $CDCl_3$) δ 158.6 (s, C=O), 62.7 (d, C-1,7), 57.1 (t, CH_2), 53.1 (d, C-8,9), 25.8 (q, NCH_3 + *t*-Bu), 18.2 (s, *t*-Bu), −5.5 (q, $SiMe_2$). Anal. Calcd for $C_{21}H_{41}O_4N_3Si_2$: C, 55.34; H, 9.07; N, 9.22. Found: C, 55.46; H, 8.94; N, 9.13.

exo,exo-8,9-Bis(hydroxymethyl)-4-methyl-2,4,6-triazatricyclo-[5.1.1.0^{2,6}]nonane-3,5-dione (15). To a solution of 12.4 g (27.2 mmol) of **10** in 50 mL of THF was added a solution of 22.3 g (70.7 mmol) of tetra-*n*-butylammonium fluoride trihydrate in 85 mL of THF.[101] After 40 min the orange solution was poured into 200 mL of ether atop a 10 cm × 2.5 in. silica column. The sample was loaded onto the column and flash chromatographed with 2 L of 3:1 (v/v) ether/methanol eluant to afford an orange oil. This was flash chromatographed on a 10 cm × 5 in. ether-packed silica column with 3:1 ether/methanol. The resulting cloudy material was dissolved in THF, filtered by suction through a fine frit, and concentrated under vacuum to 6.2 g of extremely viscous, slightly yellow syrup, which by ^{1}H NMR contained 5.40 g (87.5%) of **15** (R_f = 0.45) and residual tetrabutylammonium contaminant. Crystallization of this material can usually be induced by removal of the last traces of solvent. Further chromatography provides higher purity colorless product; however, the material is typically carried forward without further purification. Preparative TLC (silica, Et$_2$O/MeOH) provided a spectroscopic sample: ^{1}H NMR (400 MHz, acetone-d_6) δ 4.69 (t, $J_{1,8}$ = 1.7 Hz, 2 H, H-1,7), 3.79 (t, J = 5.4 Hz, 2 H (variable integration; D_2O-exchangedable), OH), 3.30 (dd, $J \simeq 6$ Hz, 4 H, CH_2), 2.92 (s, 3 H, NCH_3), 2.52 (tt, J = 1.7, 6.4 Hz, 2 H, H-8,9).

exo,exo-8,9-Bis[[(2-nitrophenyl)seleno]methyl]-4-methyl-2,4,6-triazatricyclo[5.1.1.0^{2,6}]nonane-3,5-dione (17). Diol **15** (2.70 g, 11.9 mmol) was dissolved in 150 mL of dry THF, 13.6 g (59.9 mmol) of *o*-nitrophenyl selenocyanate [prepared by literature methods[40a,105] and purified by flash chromatography (silica, CH_2Cl_2)] followed by trituration with ether to provide crystalline yellow-orange solid] was added, and the mixture was cooled to 0 °C. With magnetic stirring under a nitrogen atmosphere, 15.3 mL (12.4 g, 61.4 mmol) of tri-*n*-butylphosphine[106] was added via syringe over ca. 5 min, turning the slurry dark red. After 40 h at room temperature the THF was removed completely by rotary evaporation. The remaining material was dissolved in CH_2Cl_2 (ca. 60 mL), silica was added, and the solvent was removed, leaving a sticky, solid material. This was applied to a 10 cm × 4.5 in. silica column and flash chromatographed with 2 L of CH_2Cl_2 followed by 1.5 L of 9:1 (v/v) CH_2Cl_2/ether eluent to furnish an orange solid. Trituration with $CHCl_3$/ether afforded 4.25 g (60%) of **17** (R_f = 0.5 in 9:1 CH_2Cl_2/Et$_2$O) as a yellow solid. An additional trituration provided an analytical sample: UV-vis (CH_2Cl_2) λ_{max} 256 nm (ϵ 26 800), 390 (ϵ 7420); ^{1}H NMR (400 MHz, $CDCl_3$) δ 8.27 (d, 2 H, ArH), 7.54, 7.40, 7.34 (pseudo-t, d, pseudo-t, 6 H, ArH), 4.77 (t, J = 1.7 Hz, 2 H, H-1,7), 3.07 (s, 3 H, NCH_3), 2.69 (d, J = 7.1 Hz, 4 H, CH_2), 2.53 (tt, J = 1.7, 7.1 Hz, 2 H, H-8,9). Anal. Calcd for $C_{21}H_{19}O_6N_5Se_2$: C, 42.37; H, 3.22; N, 11.76. Found: C, 41.74; H, 3.15; N, 11.40.

8,9-Dimethylene-4-methyl-2,4,6-triazatricyclo[5.1.1.0^{2,6}]nonane-3,5-dione (18). Selenide **17** (4.25 g, 7.14 mmol) was dissolved in 900 mL of $CHCl_3$, and the solution was cooled to −60 °C. With magnetic stirring, a stream of O_3 in oxygen (ca. 0.8 mmol of O_3 min^{-1}) was bubbled into the solution for 22 min (17.6 mmol), causing it to acquire a blue color. The excess ozone was purged with a stream of N_2 and 5.0 mL (3.61 g, 35.7 mmol) of diisopropylamine was added. In a dry 5-L three-necked round-bottomed flask equipped with an inlet-topped condenser and a septum were placed 2 L of CCl_4 and 5.0 mL of *i*-Pr$_2$NH (distilled from KOH), and the solution was stirred magnetically and heated to reflux under N_2. To this was added the cold selenoxide solution[107] via a cannula over 1.5 h, and the resulting orange solution was allowed to cool after another 15 min. The solution was split into two portions, and each was washed with 5% HCl (500 mL), 5% Na_2CO_3 (500 mL), and brine (50 mL), dried over $MgSO_4$, and concentrated by rotary evaporation to an oily, orange-red paste. This was flash chromatographed on two 1:1 charcoal/Celite columns: the first, a 5 cm × 4.5 in. (90-g) column with 400 mL of CH_2Cl_2 as eluent; the second, a 5 cm × 3 in. (60-g) column with 250 mL of CH_2Cl_2. Removal of the solvent provided a yellow-orange solid which was flash chromatographed on a 5 cm × 6.5 in. silica column with 1.5 L of 1:1 (v/v) petroleum ether/ether eluent to afford **18** (R_f = 0.25) as a slightly yellow solid. This was triturated with ether/pentane (1.5 mL of each) to provide a white solid (0.90 g, 66%). Recrystallization from CH_2Cl_2/hexane furnished an analytical sample: mp ca. 152 °C dec; ^{1}H NMR (400 MHz, $CDCl_3$) δ 5.024, 5.019 (2 s, 6 H, H-1,7, =CH_2), 3.04 (s, 3 H, NCH_3); ^{1}H NMR (400 MHz, C_6D_6) δ 4.48 (s, 2 H, H-1,7), 4.35 (s, 4 H, =CH_2), 2.49 (s, 3 H, NCH_3); ^{13}C NMR (100 MHz, C_6D_6) δ 161.6 (C=O), 138.2 (C-8,9), 100.1 (=CH_2), 69.3 (C-1,7), 25.7 (NCH_3). An INEPT experiment provided J_{CH} (bridgehead) = 189 Hz, J_{CH} (=CH_2) = 164 Hz; IR (CH_2Cl_2) 3060 (w), 2940 (w), 1775 (m), 1720 (s), 1445 (m), 1390 (m), 1220 (w), 1165 (m), 1080 (w), 1015 (m), 980 (w), 910 (m), 810 (m) cm^{-1}; UV (MeOH) λ_{max} 210 nm (ϵ 16 800); MS (EI) *m/e* (relative intensity) 191 (36, M^+), 134 (35, $M^+ - CH_3NCO$), 106 (33, $M^+ - CH_3NCO$, CO), 79 (34), 78 (55, $M^+ - CH_3NCO$, CO, N_2), 77 (29), 65 (33), 64 (29), 52 (100). Anal. Calcd for $C_9H_9O_2N_3$: C, 56.54; H, 4.74; N, 21.98. Found: C, 56.50; H, 4.72; N, 21.87.

5,6-Dimethylene-2-(*N*-methylcarbamoyl)-2,3-diazabicyclo[2.1.1]hexane (19). To a solution of 0.300 g (1.57 mmol) of **18** in 24 mL of 6:1 (v/v) DMSO/water was added 87% KOH (0.360 g, 5.58 mmol), and the solution was stirred under N_2.[42] After 2 h the solution was acidified with 5% HCl (pH 2–3), causing gas evolution. After another hour ca. 15 mL of saturated aqueous $NaHCO_3$ was added, followed by enough water to dissolve the precipitated solid, and the product was extracted with $CHCl_3$ (6 × 30 mL) and dried over $MgSO_4$. The $CHCl_3$ was removed by rotary evaporation and the residual DMSO (ca. 15 mL) by distillation (bath temperature 45 °C/<1 mm). The residue was taken up in CH_2Cl_2, applied to a silica preparative-TLC plate (20 cm square × 2 mm thick), and eluted three times with ether. Semicarbazide **19** (R_f = 0.25–0.40) was recovered with 50 mL of 1:1 (v/v) petroleum ether/THF followed by 50 mL of THF, and the solvent was removed under vacuum in subdued light (ca. 24 h) to afford 0.234 g (90%) of slightly yellow, extremely viscous syrup (stored under N_2 at −30 °C). Low-temperature NMR data are reported here because a slow inversion at the amine center broadens the olefinic ^{13}C peaks and causes some ambiguity in the olefinic proton resonances (e.g., 3:1 peak ratios in some solvents): ^{1}H NMR (400 MHz, CD_2Cl_2, −60 °C) δ 6.42 (br q, 1 H, amide NH), 4.97 (d, J = 5.4 Hz, 1 H, amide-bridgehead CH), 4.789, 4.785, 4.776, 4.759 (4 s, 1 H each, =CH_2), 4.39 (br s, 1 H, amine NH), 4.32 (d, J = 5.4 Hz, 1 H, amine-bridgehead CH), 2.70 (d, J = 4.9 Hz, NCH_3); ^{13}C NMR (100 MHz, CD_2Cl_2, −60 °C) δ 162.9 (C=O), 141.8, 138.4 (quat), 97.0, 95.4 (=CH_2), 66.8, 65.1 (CH), 26.4 (NCH_3); IR (CH_2Cl_2) 3410 (m), 3270 (w), 3040 (w), 2940 (w), 1670 (s), 1520 (s), 1410 (w), 1370 (w), 1260 (w), 1210 (w), 1155 (w), 1110 (w), 1045 (m), 960 (w), 915 (m), 900 (m), 835 (w), 810 (w), 790 (w) cm^{-1}. An additional preparative TLC provided an analytical sample. Anal. Calcd for $C_8H_{11}N_3O$: C, 58.17; H, 6.71; N, 25.44. Found: C, 57.60; H, 6.69; N, 25.03.

Nickel peroxide was prepared by the method of Nakagawa et al.,[108] which provides material with an activity (determined titrimetrically[108]) of ca. 3.5 mmol of "available oxygen" (aO) per gram. We have found this oxidant to be unsuitable for our purposes. However, reactivation[45,108] of this substance with NaOCl yields a solid that can be filtered much more rapidly (with less exposure to air) than the original material and (after thorough drying under vacuum) has an activity of at least 4.5 mmol of aO g^{-1}. We have obtained variable results with nickel peroxide that has been stored for more than a few days at −30 °C. After a considerable amount of experience we have concluded that the only foolproof way to ensure the success of the oxidation of **19** is to use freshly made and freshly reactivated oxidant. The reactivation procedure is as follows. To 4 g of ground, dried nickel peroxide was added 40 mL of 5% sodium hypochlorite solution (Aldrich), with a resultant evolution of gas. The black slurry was stirred for 30 min, then filtered by suction, and washed three times with 20 mL of water. The black filter cake was then dried under vacuum for 48 h and ground to a find powder.

2,3-Diaza-5,6-dimethyleneblcyclo[2.1.1]hex-2-ene (2). In a dry solid addition ampule was placed 500 mg (2.25 mmol of aO) of fresh nickel peroxide, and the ampule was fitted to a dry 25-mL pear-shaped flask equipped with a septum. The assembly was flushed with argon, ca. 6 mL of CH_2Cl_2 was introduced and cooled to −78 °C, and the nickel peroxide was added to the flask. A solution of 25 mg (0.15 mmol) of the semicarbazide (**19**) in ca. 7 mL of CH_2Cl_2 (distilled from CaH_2 under N_2) was placed in a dry 10-mL flask and cooled to −78 °C under positive pressure of argon. With efficient magnetic stirring, the cold semicarbazide solution was added to the nickel peroxide slurry via 30-gauge

(105) Bauer, H. *Chem. Ber.* **1913**, *46*, 92–98.
(106) Grieco, P. A.; Gilman, S.; Nishizawa, M. *J. Org. Chem.* **1976**, *41*, 1485–1486.
(107) Reich, H. J.; Renga, J. M.; Reich, I. L. *J. Am. Chem. Soc.* **1975**, *97*, 5434–5447.
(108) Nakagawa, K.; Konaka, R.; Nakata, T. *J. Org. Chem.* **1962**, *27*, 1597–1601.

Teflon tubing over ca. 5 min. (The reaction was typically analyzed for remaining semicarbazide by TLC.) A sample was obtained by filtering an aliquot through a plug of glass wool resting against a constriction in a piece of 20-gauge Teflon tubing. If insufficiently active nickel peroxide had been used, more could be added at this point and the reaction time increased accordingly. The reaction was normally allowed to continue for 30 min to 1 h. A separate assembly was constructed with warm glassware. This consisted of a 25-mL pear-shaped flask with a high-vacuum valve and a septum-capped sintered glass frit. The frit was equipped with a cooling jacket and a gas inlet arm having a stopcock. While the apparatus was warm, a ca. 1.5-cm pad of Celite was placed on the frit and covered with a small piece of glass wool. The frit and flask were connected through a *y* joint to a source of argon and aspirator vacuum. When the reaction was judged to be complete, the frit and flask were cooled to −78 °C, the Celite pad was moistened with ca. 2 mL of CH_2Cl_2, and the slurry was cannulated through a judiciously short piece of 20-gauge Teflon tubing into the frit assembly. The solution was filtered, the Celite pad was rinsed with another ca. 2 mL of CH_2Cl_2, and the solvent was removed (to a liquid N_2 trap) at −78 °C under vacuum in subdued light over the course of several hours to afford the title diazene **2** as a white solid. (An early sample of a few milligrams of **2** decomposed explosively, possibly due to overexposure to air and/or light; we have since experienced no difficulty in handling milligram quantities of the pure diazene). We use this material without further purification; attempts at recrystallization have generally failed to increase the purity of the sample, but only decrease the yield. We also note that methylene chloride appears to be by far the best solvent for crystalline diazene **2**. This material is only slightly soluble in the other solvents commonly used (e.g., MTHF). Solutions of **2** in these solvents were made either by first dissolving the crystalline solid in a minimal amount of methylene chloride or by dissolving diazene that had not yet crystallized (or by dissolving impure material): ^{1}H NMR (400 MHz, CD_2Cl_2, −80 °C) δ 5.48 (s, 2 H, CH), 4.75 (s, 4 H, CH_2); ^{1}H NMR (400 MHz, C_7D_8, −80 °C): δ 4.66 (s, 2 H, CH); 4.07 (s, 4 H, CH_2); ^{13}C NMR (22.6 MHz, CD_2Cl_2, −75 °C) δ 157.7, 97.0, 82.9. These signals were found to vanish upon warming the sample to −50 °C, in accord with the thermal loss of the proton signals. The yield of the reaction was determined by ^{1}H NMR. Thus, the best diazene samples were found to contain 80–85% **2** and 15–20% dimers (**21** and **22**), for an overall reaction yield of ca. 30%: UV (MTHF) λ_{max} 333 nm, ca. 320 (sh) UV (CD_2Cl_2) λ_{max} 331 nm, ca. 320 (sh). The samples invariably displayed a large absorption extending up to ca. 280 nm. This is not due to **2**, and it presumably arises from the dimeric decomposition products. The ϵ of the diazene in CD_2Cl_2 was determined by making several UV absorbance measurements and determining the concentration of **2** by NMR. Thus, three such measurements provided ϵ = (0.146 (±0.001))/(0.35 (±0.01) cm)(1.80 (±0.2) × 10^{-3} M) = 230 (±30) M^{-1} cm^{-1}, ϵ = (0.157 (±0.001))/(0.35 (±0.01) cm)(1.86 (±0.2) × 10^{-3} M) = 240 (±30) M^{-1} cm^{-1}, and ϵ = (0.303 (±0.02))/(0.35 (±0.01) cm)(3.69 (±0.2) × 10^{-3} M) = 240 (±20) M^{-1} cm^{-1}, for an average of 240 M^{-1} cm^{-1}.

***endo*,*endo*-2,4-Bis[(*tert*-butyldimethylsiloxy)methyl]bicyclo[1.1.0]butane-*1,3*-d_2 (7-d_2).** A stirred solution of the bicyclobutane (2.40 g of impure material estimated to contain 1.80 g of **7**, 5.25 mmol) in 7 mL of dry ether, under argon, was cooled in an ice bath. To this was added 14.5 mL of a 1.45 M solution of *n*-butyllithium (21.0 mmol) in hexane[53] via syringe over ca. 5 min, and the orange solution was stirred at room temperature for 6.5 h. The solution was then cooled to 0 °C and quenched by the cautious addition of excess D_2O (1.1 mL, 55 mmol), and the resultant mixture was allowed to warm. The solution was dried (Na_2SO_4) and concentrated under vacuum. This procedure was repeated two more times to afford 1.70 g of 7-d_2 as a dark orange liquid. This was judged to be acceptably pure by ^{1}H NMR, the spectrum corresponding to that of **7** but lacking the signal of and splitting produced by the bridgehead protons. This material was carried forward without further purification.

2,3-Diaza-5,6-dimethylenebicyclo[2.1.1]hex-2-ene-*1,4*-d_2 (2-d_2). Bicyclobutane 7-d_2 was subjected to the standard reaction sequence (see above). ^{1}H NMR spectra of the intermediate compounds were consistent with bridgehead deuteration. In addition, a mass spectrum of **18**-d_2 displayed a series of peaks corresponding exactly to those assigned (above) to **18** (M^+) and the intermediates generated by the sequential fragmentation of the urazole moiety, at m/e + 2 relative to those of **18**; specifically, m/e 193 (100), 136 (91), 108 (62), 80 (89), 66 (8), 65 (9), 53 (12), 40 (4). A high-quality ^{1}H NMR spectrum (400 MHz, CD_2Cl_2) of 2-d_2 allowed an estimate of the extent of deuterium incorporation. The signal of the residual bridgehead protons was only slightly larger than the ^{13}C satellites of the olefinic signal, indicating that the three cycles of *n*-BuLi/D_2O exchange had replaced >99% of the bridgehead hydrogens of **7**.

Curie Plot. A sample of **2** in 1:1 EtOH/MeOH[68] was placed in the EPR cavity at 4 K, irradiated with light from the Hg(Xe) arc lamp using filter combination no. 2 (Table I) and the cavity was shrouded against stray light. The sample was then warmed to 70–80 K for 15 min to allow decay of any biradicals in "fast" matrix sites. The temperature was then lowered in 3–6 °C increments and allowed to stabilize for several minutes at each temperature. The indicated (TC) temperature generally fluctuated no more than ±0.1 °C during the 2-min scan. All spectra were recorded at 0.01 mW. The onset of saturation was not determined in this run due to our inability to measure the power with sufficient accuracy to generate a quantitatively meaningful intensity vs $P^{1/2}$ plot, however previous such measurements indicated that this point is ca. 15 K. Because the spectral shape was invariant with temperature, and double integration of the spectra had previously been found to cause no deviation from linearity in the Curie plot, the reported signal intensity is simply the sum of the intensities of the four *y* and *z* peaks of the first-derivative spectrum (Figure 1). Spectra were recorded as the temperature was first decreased, then increased, and then decreased again. Anomalous cryostat vacuum readings during measurement of half of the spectra in the first temperature progression and a corresponding break in the plot provided justification for rejecting this entire set. Thus, the points presented in Figure 3 represent increasing, then decreasing temperature data.

Absorption Spectrum of 1. A sample of **2** in MTHF was irradiated with monochromatic 334 (±10) nm light from a 1000-W Xe arc lamp at 77 K for 1.5 h to provide the spectrum of Figure 4; measured peak positions (nm): 505.7 (abs ≃ 2), 490.3, 469.5, 456.4, 443, 439, 426.8, 415, 401. (Spectroscopic samples were effectively opaque below ca. 280 nm, as mentioned above under the characterization of **2**.)

Fluorescence and Excitation Spectra of 1. Samples of **2** in MTHF were irradiated with monochromatic 334 (±10) nm light from a 1000-W Xe arc lamp at 77 K for 1 h to produce an intense yellow-orange color. The emission spectrometer[109] employed a 150-W Xe arc lamp as the excitation source. The spectrum of Figure 4 was recorded with 1.25-mm excitation slits and 2-mm emission slits. The excitation wavelength was 440–445 nm, and a 446-nm cutoff filter protected the PM tube from reflected light. The emission monochrometer had been calibrated to the Hg spectral lines, and the wavelength scale was corrected accordingly. The spectrum was also corrected for the variation in the response of the PM tube with wavelength; measured peak positions (nm): 510, 526, 543, 553, 574, 595, 606, 631. The excitation spectrum was recorded with 1.25-mm excitation and 5-mm emission slits. The emission was monitored at 552 nm and the wavelength scale was arbitrarily shifted 5 nm to compensate for miscalibration of the excitation monochrometer. The spectra are not corrected for the biradical decay (ca. 40%) that occurred during the scan.

Decay Rate of 1 at 77 K by EPR. A sample of **2** in MTHF was placed in the liquid N_2 filled finger Dewar in the EPR cavity, the room lights were dimmed, and the cavity area was shrouded with black cloth. The sample was photolyzed for 15 s with light from the 1000-W Hg(Xe) arc lamp directed through filter combination no. 1 (Table I). The rise and decay of the signal were monitored at 3150 G (low-field *z* transition; 9.26 GHz) with 0.5-mW microwave power. The base line was periodically checked for drift by switching to 2150 G, and the intensity measurements were corrected accordingly. The signal intensity was followed for 1.5 h, during which time ca. 15% of the signal decayed. The slope of a 20-point ln *I* vs $t^{1/2}$ plot was 2.3 (±0.5) × 10^{-3} $s^{-1/2}$ corresponding to a most probable rate constant of 9 (±4) × 10^{-7} s^{-1}.[69]

Decay Rate of 1 at 77 K by UV-vis. The sample used in the EPR experiment above was thawed and refrozen in liquid N_2. The sample was irradiated for 15 s with the 1000-W Hg(Xe) arc lamp and filter combination no. 1 (Table I) and quickly transferred to the finger Dewar, which had been mounted in the beam of the HP diode array spectrophotometer. The room lights were kept off, the sample area was shrouded with black cloth, and streams of nitrogen were directed at the outer surface of the finger Dewar to prevent condensation in the path of the light beam. A 340-nm cutoff filter was placed in front of the light source to prevent photolysis of **2** (photolysis of **1** had been found to be negligible under the conditions used), and spectra were recorded with 0.1-s measurement time and stored on disk. The intensity was measured at each of the four prominent peaks of the spectrum (Figure 4) relative to a (sloping) base line drawn between the edges of the spectrum with the aid of a program written for the HP 85A. Spectra were recorded over 4 h during which ca. 20% of the **1** initially present decayed. Data acquired during the first 30 min displayed a large amount of scatter, presumably due to some movement of the sample before it froze in place. A ln *I* vs $t^{1/2}$ plot of the remaining data for the 506-nm peak had a slope of 1.9 (±0.3) × 10^{-3} $s^{-1/2}$, corresponding to a most probable rate constant

(109) Rice, S. F.; Gray, H. B. *J. Am. Chem. Soc.* **1983**, *105*, 4571–4575.

Table II. Determination of ϵ for Triplet **1**

meas	abs (506 nm)[a]	double integral[b]	[1],[c] M	ϵ,[c] M^{-1} cm^{-1}
1 UV-vis	0.575 ± 0.03			7820 ± 1600
1 EPR		366 ± 18	2.10 (±0.25) × 10^{-4}	
2 EPR		344 ± 17	1.98 (±0.24) × 10^{-4}	6100 ± 1000
2 UV-vis	0.423 ± 0.005			
3 EPR		253 ± 30	1.45 (±0.27) × 10^{-4}	7760 ± 1800
3 UV-vis	0.394 ± 0.004			

[a] The reported errors are standard deviations. [b] The reported errors represent ±5% except for the third, which reflects the disparity of the two measurements that were averaged. [c] The errors are the sums of the relative errors in the contributing values and thus represent conservative limits.

of 6 (±2) × 10^{-7} s^{-1}.[69] Rates measured with the other vibronic peaks were all within or near this range.

Photochemical Action Spectrum. A sample of **2** in MTHF was placed in the Oxford cryostat. The sample was cooled to 4 K, and photolyzed with 334-nm light from the 1000-W Xe arc lamp (ca. 20-nm monochrometer band pass) for 5-10 min to generate a sufficient concentration of **1**. The signal intensity was monitored at 3073 G (9.27 GHz, 0.5 mW) while the monochrometer wavelength was advanced 1 nm every 10 s with the slits set for a 2.75-nm band pass. The data were recorded digitally with a resolution of ca. 5.5 points nm^{-1}. With the aid of a FORTRAN program written for the IBM-PC/AT the curve was smoothed over a 25-point region by a least-squares procedure[110] and then differentiated by using a 35-point window, which also accomplished a second least-squares smoothing.[110] The lamp intensity correction was applied as a Gaussian function of lamp intensity data with a 2.5-nm fwhm to approximate the band pass, centered at each data point. The action spectrum of Figure 5 (a and b) was shifted by ca. 2 nm (into alignment with the absorption spectrum of Figure 5c) to compensate for an apparent miscalibration of the monochrometer (possibly caused by a slight misalignment of the optical arrangement). Attempts were made to detect a second biradical transition[3d] by scanning down to 260 nm (the practical limit for the Xe lamp used) but no decay of the EPR signal was observed.

Determination of Oscillator Strength. A sample of **2** in MTHF in a standard 5-mm-o.d. EPR tube was irradiated at 77 K for ca. 7 min with light from the 1000-W Xe arc lamp that had been directed through filter combination no. 1 (Table I). The sample tube was placed well away from the optical focal point and rotated during the photolysis to provide a uniform distribution of **1** throughout the MTHF matrix. The sample was stored at 77 K for 3 h prior to the analysis in order to avoid the faster portion of the nonexponential decay (see above). The effective path length of the EPR tube in the UV-vis spectrophotometer beam was measured as 0.35 ± 0.01 cm (roughly in accord with the inner diameter specified by the manufacturer) by comparison of a standard solution's absorbance in the tube with that in an ordinary 1-cm cell. The volume contraction of the solvent was measured as ca. 20% upon cooling from room temperature to 77 K. The EPR spin standard[111] consisted of a 5.48 × 10^{-4} M solution of 2,2,6,6-tetramethylpiperidinyloxy (TEMPO) in MTHF in a tube identical with that containing the biradical sample. The concentration at 77 K was 6.85 (±0.4) × 10^{-4} M, the estimated error being based primarily upon the uncertainty in the volume change. EPR spectra were recorded at 77 K by using 0.01-mW power for TEMPO spectra and both 0.01 and 0.1 mW for spectra of **1**, thereby avoding signal saturation in both cases. The digitized first-derivative spectra were numerically double-integrated by standard methods and scaled to a common receiver gain. The 506-nm absorbance of the sample was determined by recording five spectra as the sample tube was rotated in the finger Dewar with respect to the spectrophotometer beam. The absorbance was measured relative to a base line drawn between the edges of the spectrum with the aid of an HP-85A program. Three pairs of EPR and absorption measurements were made, at ca. 3, 6, and 9.5 h after photolysis (see Table II). The second member of the pair followed the first as closely as temporospacial constraints permitted, and the order of the two was reversed to compensate for the effects of both intrinsic and adventitious decay of the biradical. Absorbance values and double integrals for the three pairs of measurements on the sample of **1** are reported in Table II. The average of the three values for ϵ is 7200 M^{-1} cm^{-1}.

Magnetophotoselection. The photolysis setup consisted of, in series, the 1000-W Hg(Xe) arc lamp, the monochrometer, and two quartz lenses having 100- and 175-mm focal lengths. The first of these was adjusted to provide a parallel light beam and the second to reduce the image of the monochrometer exit slit to approximately the width of the sample at the point of incidence. An Oriel Model 27340 polymer sheet type near-UV/visible linear polarizer was placed between the two lenses and positioned appropriately with a rotatable mount. The monochrometer was found to polarize the light somewhat in the horizontal ($\mathbf{E}\|\mathbf{H}_0$) direction; therefore, for photolyses with unpolarized light, the assembly was replaced with the standard one, in which the (unpolarized) lamp output is directed through an appropriate series of filter glasses and focused into the EPR cavity. Spectra were recorded with 0.2-mW microwave power at ca. 9.25 GHz.

Acknowledgment. We thank the National Science Foundation for generous support of this work.

(110) Savitzky, A.; Golay, M. J. E. *Anal. Chem.* **1964**, *36*, 1627-1639.

(111) When using a doublet signal as an intensity standard for a triplet, one must include a correction for the fact that triplet signals are inherently $^4/_3$ as intense per electron as doublet signals, or $^8/_3$ as intense per paramagnet. See, for example: Platz, M. S.; Berson, J. A. *J. Am. Chem. Soc.* **1980**, *102*, 2358-2364.

2,4-Dimethylenebicyclobutane: Preparation, Characterization, and Relationship to the Non-Kekulé Isomer of Benzene

Gary J. Snyder[1] and Dennis A. Dougherty*

Contribution No. 7847 from the Arnold and Mabel Beckman Laboratory of Chemical Synthesis, California Institute of Technology, Pasadena, California 91125. *Received September 22, 1988*

Abstract: Thermolysis or direct photolysis of 5,6-dimethylene-2,3-diazabicyclo[2.1.1]hex-2-ene (**2**) in fluid solution produces 2,4-dimethylenebicyclo[1.1.0]butane (**3**), whose ^{1}H NMR spectrum (-80 °C, CD_2Cl_2) consists of singlets at δ 4.22 and 3.18 in a 2:1 ratio. Compound **3** is thermally unstable and dimerizes with second-order kinetics between -80 and -25 °C ($\Delta H^{\ddagger}$ = 6.8 kcal/mol, $\Delta S^{\ddagger}$ = -28 eu) by a novel mechanism involving direct combination of two molecules of **3** in the rate-determining step. This singlet-manifold reaction ultimately produces a mixture of two dimers, 3,8,9-trimethylenetricyclo[5.1.1.$0^{2,5}$]non-4-ene (**11**) and *trans*-3,10-dimethylenetricyclo[6.2.0.$0^{2,5}$]deca-4,8-diene (**12t**), with the former predominating. In contrast, triplet-sensitized photolysis of **2**, which leads to triplet 2,4-dimethylene-1,3-cyclobutanediyl (**1**), provides in addition to **11** and **12t**, a substantial amount of *trans*-5,10-dimethylenetricyclo[6.2.0.$0^{3,6}$]deca-3,8-diene (**13t**) and small amounts of two unidentified dimers. In addition, triplet biradical **1** ring closes to **3** in rigid media both thermally (77-140 K) and photochemically. In solution, **3** forms triplet **1** upon energy transfer from sensitizers having relatively low triplet energies. The implications of the thermal chemistry for the energy surfaces of the system are discussed.

In the preceding paper[2] we described the preparation of the non-Kekulé isomer of benzene, 2,4-dimethylene-1,3-cyclobutanediyl (**1**), by photolysis of diazene **2** under cryogenic conditions in rigid media. Triplet **1** was found to be quite amenable

0002-7863/89/1511-3942$01.50/0